Atmos. Chem. Phys. Discuss., 5, 12313–12371, 2005
www.atmos-chem-phys.org/acpd/5/12313/
SRef-ID: 1680-7375/acpd/2005-5-12313
European Geosciences Union

Atmospheric Chemistry and Physics Discussions

Peroxy radical chemistry and the control of ozone photochemistry at Mace Head, Ireland during the summer of 2002

Z. L. Fleming[1], P. S. Monks[1], A. R. Rickard[1,2], D. E. Heard[2], W. J. Bloss[2], P. W. Seakins[2], T. J. Still[2], R. Sommariva[2,*], M. J. Pilling[2], R. Morgan[2], T. J. Green[3], N. Brough[3], G. P. Mills[3], S. A. Penkett[3], A. C. Lewis[4], J. D. Lee[4], A. Saiz-Lopez[3], and J. M. C. Plane[3]

[1]Department of Chemistry, University of Leicester, Leicester, UK
[2]School of Chemistry, University of Leeds, Leeds, UK
[3]School of Environmental Sciences, University of East Anglia, Norwich, UK
[4]Department of Chemistry, University of York, UK
[*]now at: Aeronomy Lab, NOAA, USA

Received: 12 October 2005 – Accepted: 30 October 2005 – Published: 28 November 2005

Correspondence to: P. S. Monks (p.s.monks@le.ac.uk)

Abstract

Peroxy radical ($HO_2+\Sigma RO_2$) measurements, using the PEroxy Radical Chemical Amplification (PERCA) technique at the North Atlantic Marine Boundary Layer EXperiment (NAMBLEX) at Mace Head in summer 2002, are presented and put into the context of marine, boundary-layer chemistry. A suite of other chemical parameters (NO, NO_2, NO_3, CO, CH_4, O_3, VOCs, peroxides), photolysis frequencies and meteorological measurements, are used to present a detailed analysis of the role of peroxy radicals in tropospheric oxidation cycles and ozone formation. Under the range of conditions encountered the peroxy radical daily maxima varied from 10 to 40 pptv. The diurnal cycles showed an asymmetric shape typically shifted to the afternoon. Using a box model based on the master chemical mechanism the average model measurement agreement was 2.5 across the campaign. The addition of halogen oxides to the model increases the level of model/measurement agreement, apparently by respeciation of HO_x. A good correlation exists between j(HCHO).[HCHO] and the peroxy radicals indicative of the importance of HCHO in the remote atmosphere as a HO_x source, particularly in the afternoon. The peroxy radicals showed a strong dependence on [NO_x] with a break point at 0.1 ppbv, where the radicals increased concomitantly with the reactive VOC loading, this is a lower value than seen at representative urban campaigns. The $HO_2/(HO_2+\Sigma RO_2)$ ratios are dependent on [NO_x] ranging between 0.2 and 0.6, with the ratio increasing linearly with NO_x. Significant night-time levels of peroxy radicals were measured up to 25 pptv. The contribution of ozone-alkenes and NO_3-alkene chemistry to night-time peroxy radical production was shown to be on average 59 and 41%. The campaign mean net ozone production rate was 0.11 ± 0.3 ppbv h^{-1}. The ozone production rate was strongly dependent on [NO] having linear sensitivity ($d\ln(P(O_3))/d\ln(NO)=1.0$). The results imply that the $N(O_3)$ (the in-situ net photochemical rate of ozone production/destruction) will be strongly sensitive in the marine boundary layer to small changes in [NO] which has ramifications for changing NO_x loadings in the European continental boundary layer.

ACPD

5, 12313–12371, 2005

1. Introduction

Peroxy radicals (HO_2 and RO_2, predominantly CH_3O_2 in semi-polluted atmospheres) can be thought of as the intermediates between the hydroxyl (OH) radical and ozone formation or destruction (Monks, 2005). Peroxy radicals also control the removal of primary pollutants such as NO_x(NO+NO_2) and Volatile Organic Compounds (VOCs). Understanding the radical chemistry that controls ozone formation will improve our basic understanding of tropospheric photochemistry and the effect of natural and man-made emissions on ozone formation.

The relative contribution of ozone production and loss processes in the troposphere is highly sensitive to competition between the reaction of peroxy radicals with NO and their self- and cross-reactions to form peroxides. In the presence of NO_x, the reaction of peroxy radicals with NO leads to the formation of NO_2, which, upon photolysis, forms ozone:

$$HO_2 + NO \rightarrow OH + NO_2 \quad \text{(R1)}$$

$$CH_3O_2 + NO \rightarrow CH_3O + NO_2 \quad \text{(R2)}$$

$$CH_3O + O_2 \rightarrow HO_2 + HCHO \quad \text{(R3)}$$

$$NO_2 + h\nu\ (\lambda < 424\,\text{nm}) \rightarrow O(^3P) + NO \quad \text{(R4)}$$

$$O(^3P) + O_2 + M \rightarrow O_3 + M \quad \text{(R5)}$$

In conditions of low [NO_x], a catalytic cycle leads to net ozone destruction, shown here for the reaction with CO:

$$HO_2 + O_3 \rightarrow OH + 2O_2 \quad \text{(R6)}$$

$$OH + CO \rightarrow H + CO_2 \quad \text{(R7)}$$

$$H + O_2 + M \rightarrow HO_2 + M \quad \text{(R8)}$$

$$\text{Overall}: CO + O_3 \rightarrow CO_2 + O_2 \quad \text{(R9)}$$

ACPD
5, 12313–12371, 2005

OH oxidation and other VOCs forms peroxy radicals:

$$CH_4 + OH \rightarrow CH_3 + H_2O \quad \text{(R10)}$$

$$CH_3 + O_2 + M \rightarrow CH_3O_2 + M \quad \text{(R11)}$$

Both urban and rural environments are affected by air pollution of photochemical origin, and the modelling of photochemical ozone formation in the British Isles from European emissions are important for the policy-makers in order to develop emission-reduction targets for ozone precursors (Metcalfe et al., 2002; Derwent et al., 2003). Ozone is one of the major components of photochemical smog, together with contributions from compounds such as carbonyls, peroxy acetyl nitrates (PANs) and various nitrogen oxides. It has been seen in past studies in the relatively clean rural/marine conditions of Mace Head (Salisbury et al., 2001, 2002) during the EASE 96 and 97 (Eastern Atlantic Summer/Spring Experiment) and in the very clean air of Cape Grim in Tasmania (Monks et al., 1998 and 2005[1]) at the SOAPEX 2 (Southern Ocean Atmospheric Photochemistry EXperiment) campaign in 1998 that ozone formation is part of a natural cycle that can be easily perturbed by pollution events.

Tropical maritime air which is depleted in ozone can be advected to Mace Head over a distance of several thousand kilometres without significant net ozone formation occurring (Derwent et al., 1998). Measurements at Mace Head found that the site experienced more photochemical ozone production than destruction during the EASE 96 and 97 campaigns (Salisbury et al., 2002) and at ATAPEX-95 (Atlantic Atmospheric Photochemistry Experiment) (Carpenter et al., 1997). Cape Grim experienced far more days with net ozone destruction as in SOAPEX 1 in 1995 (Monks et al., 1998, 2000; Carpenter et al., 1997) and in 1998 at SOAPEX 2 (Monks et al., 2005). Andres-Hernandez et al. (2001) also found that during the Atlantic and Southern Indian Ocean cruise of AEROSOL 99 that net ozone destruction predominated.

[1]Monks, P. S., Salisbury, G., Fleming, Z. L., et al.: The role of peroxy radicals in photochemical destruction of ozone at mid-latitudes in the Southern Hemisphere, in preparation, 2005.

ACPD
5, 12313–12371, 2005

Penkett et al. (1997) showed that the relationship between the sum of peroxy radicals and the ozone photolysis rate coefficient (to the singlet oxygen atom), $j(O^1D)$ can serve as a diagnostic for photochemical ozone production and destruction. In high NO_x conditions $HO_2+\Sigma RO_2$ is generally proportional to $j(O^1D)$ and in clean conditions, to $\sqrt{j(O^1D)}$ (Penkett et al., 1997; Monks et al., 1998; Zanis et al., 1999; Creasey et al., 2003). The shape of $j(O^1D)$ throughout the day produces a typical summer peroxy radical diurnal cycle with maximum values towards solar noon, and minimum values during the night. Photolysis of other photo-labile compounds (e.g. HCHO and HONO) becomes noticeable in the early morning or evening, when the light is of longer wavelengths than those at which ozone photolysis occurs, and can lead to a broader peroxy radical diurnal cycle than that expected from ozone photolysis alone.

In the absence of photochemistry, there is a series of night-time peroxy radical-producing channels. NO_3 (nitrate) radical (Allen et al., 1999; Penkett et al., 1999; Salisbury et al., 2001) and ozone reactions with alkenes (Hu and Stedman, 1995; Rickard et al., 1999; Salisbury et al., 2001) were found to be two dominant channels in the marine influenced atmosphere.

In this paper, by use of peroxy radical measurements coupled to a suite of supporting trace species measurements, the photochemical environment of Mace Head is explored. In particular, the shape, concentration and form of the diurnal cycle are explored in relation to both primary production and the potential contribution of the photolysis of secondary compounds such as carbonyls (e.g. HCHO). The dependence of peroxy radical concentration with changing NO_x and VOC is described. The role of both NO_3 and O_3-alkene reactions as night time source of peroxy radicals is investigated. Finally, role of the peroxy radicals in the in situ photochemical formation and destruction of ozone is quantified.

ACPD
5, 12313–12371, 2005

2. Experimental

2.1. Site

NAMBLEX took place from 27 July to 2 September 2002 at the Mace Head Atmospheric Research Station (53°20′ N, 9°54′ W). Mace Head is located on the west coast of Ireland, 88 km west of Galway city, and is in the path of the mid-latitude cyclones which frequently traverse the North Atlantic. Heard et al. (2005) describe the location in more detail, together with the local meteorology of the site, and Norton et al. (2005) provide a detailed analysis of the specific boundary layer conditions encountered during NAMBLEX. The prevailing wind direction is from a westerly marine sector but significant pollution events also reach the site from European continental air-masses, from easterly directions.

2.2. Peroxy radical measurements (PERCA)

Measurements of peroxy radicals ($HO_2+\Sigma RO_2$) were carried out using the jointly operated University of Leicester – University of East Anglia (UEA) PEroxy Radical Chemical Amplifier (PERCA IV) instrument, reported for the first time in Green et al. (2005)[2] and Fleming et al. (2005)[3]. The technique was pioneered by Cantrell et al. (1984) and described by Clemitshaw et al. (1997), Monks et al. (1998) and Green et al. (2003) and the current apparatus uses a dual channel inlet and detection system (as in Cantrell et al., 1996).

[2]Green, T. J., Reeves, C. E., Fleming, Z. L., Brough, N., Rickard, A. R., Bandy, B. J., Monks, P. S., and Penkett, S.A.: An improved dual channel PERCA for atmospheric measurements of peroxy radicals, J. Environ. Monitoring, in review, 2005.

[3]Fleming, Z. L., Monks, P. S., Rickard, A. R., Bandy, B. J., Brough, N., Green, T. J., Reeves, C. E., and Penkett, S. A.: Seasonal dependence of peroxy radical concentrations at a Northern hemisphere marine boundary layer site during summer and winter: evidence for photochemical activity in winter, Atmos. Chem. Phys. Discuss., in preparation, 2005b.

ACPD
5, 12313–12371, 2005

Briefly, the method relies upon the HO_2 and OH radical-catalysed conversion of NO and CO into CO_2 and NO_2 respectively, through addition of NO and CO into the inlet region *viz.*,

$$HO_2 + NO \rightarrow OH + NO_2$$
$$OH + CO \rightarrow H + CO_2$$
$$H + O_2 + M \rightarrow HO_2 + M$$
$$\text{Overall} : NO + CO + O_2 \rightarrow CO_2 + NO_2 \quad \text{(R12)}$$

Organic peroxy radicals are readily converted into HO_2 in the presence of NO with varying efficiencies (Ashbourn et al., 1998). The yield of both CO_2 and NO_2 is equal to CL×([RO_2]+[HO_2]+[OH]), where CL is the chain length, i.e. the number of HO_2/OH inter-conversion cycles that occur before radical termination. The ratio of [HO_2]/[OH] ranges from ∼50–200 in the atmosphere, therefore the PERCA technique effectively measures the sum of inorganic and organic peroxy radicals. The yield of NO_2 is measured using commercial LMA-3 detectors (calibrated daily using NO_2 permeation sources) and this is converted into [HO_2+ΣRO_2] using Δ[NO_2]/CL. The chain length was calculated on a weekly basis, using a calibration source based upon the photolysis of CH_3I at 253.7 nm to yield CH_3O_2 at varying concentrations (Clemitshaw et al., 1997).

Background [NO_2] signals (caused by the reaction of ambient ozone with NO in the inlet) were measured by changing the addition points of the reagent gases, so that the amplification reactions are not initiated. The overall radical levels are calculated by subtracting the termination signal from the amplification signal.

The dual-inlet system comprises two distinct sampling systems, inlet reaction sites and detectors. The advantage of this dual-inlet system is that the two systems are run out of phase in two modes, with one in amplification and the other in termination mode. Switching the two inlets between phases on a minute time scale leads to a continuous amplification and termination signal.

Mihele et al. (1998, 1999) have shown that the chain length of a chemical ampli-

fier is reduced in the presence of atmospheric water vapour (see also Reichert et al., 2003). Salisbury et al. (2002) demonstrated that the chain length of the Leicester-UEA PERCA instrument falls approximately linearly with increasing specific humidity. From a series of laboratory experiments, a humidity correction factor equation (using ambient humidity and inlet temperatures) was derived and applied to all PERCA data. In order to minimise the applied correction factor, the inlet temperature was kept above ambient temperatures at the constant value of 30°C. The humidity correction factor varied between 1.5 and 2.5 during NAMBLEX (see also Fleming et al., 2005b[3]).

The accuracy and precision of the dual-inlet PERCA have been assessed in detail by Fleming (2005a). The overall uncertainty for any give peroxy radical measurement is 38% (at 1σ) from a combination of uncertainties associated with the radical calibration, NO_2 quantification and humidity correction. The precision on a 1 pptv measurement averaged over a minute assessed from the reproducibility of the radical calibration was 15%. The detection limit of the instrument was of the order of 0.5 pptv at a S/N of 1 on a 1 min average.

The PERCA instrument inlet box was securely attached 6 m above ground level to a tower on a temporary laboratory building (sea container) close to the main shoreline site and an umbilical line carried the reagent gases and sample lines down to the main rack in the laboratory (see Heard et al., 2005, for a site plan). The PERCA instrument took measurements continuously during the campaign in minute averages and analysis was carried out with ten minute- or hourly-averaged data.

2.3. Other measurements

Meteorological data were obtained from the site's fixed meteorological station, which recorded ambient air temperature, relative humidity, wind speed and wind direction. The other instruments were housed in the permanent cottages of the site or in similar self-contained temporary buildings (sea-containers). Details of the instruments, their detection limits and accuracy are given in Heard et al. (2005).

2.4. Modelling studies

The Master Chemical Mechanism (currently MCMv3.1, available online at http://mcm.leeds.ac.uk/MCM/) Developed by Jenkin et al. (1997) and subsequently refined and updated by Saunders et al. (2003), Jenkin et al. (2003) and Bloss et al. (2005a and b). MCMv3.1 contains the oxidation mechanisms of 135 primary emitted VOCs. This mechanism was added to a campaign optimised box model used to simulate HO_2, RO_2 and OH radical concentrations constrained with H_2, CO, CH_4, O_3, NO, NO_2, HCHO, measured VOCs, chloroform, temperature and various photolysis rates measurements. In general, the most complete model shown in this analysis is termed "full-oxy" and is detailed extensively in Sommariva et al. (2005a). The model was constrained to CO, CH_4, 23 hydrocarbons, 3 oxygenates and 2 peroxides and to temperature and photolysis measurements. OH and HO_2 model/measurement comparisons are reported in Smith et al. (2005), Sommariva et al. (2005a) and night-time HO_2 and RO_2 in Sommariva et al. (2005b)[4]. Model results at NAMBLEX for HO_2 were in much better agreement with the measurements when the model was additionally constrained to measured halogen oxides (Sommariva et al., 2005a; Bloss et al., 2005c).

3. Results

3.1. Meteorological conditions

Local wind speed and direction measurements were recorded on an hourly basis during NAMBLEX. During the EASE campaigns Salisbury et al. (2002) and Rickard et al. (2002) divided all the data into five sectors, according to local wind direction.

[4]Sommariva, R., Ball, S. M., Bitter, M., Bloss W. J., Fleming, Z. L., Heard, D. E., Jones, R. L., Lee, J. D., Monks, P. S., Pilling, M. J., Plane, J. M. C., and Saiz-Lopez, A.: Night-time radical chemistry during the NAMBLEX campaign, Atmos. Chem. Phys. Discuss., in preparation, 2005b.

ACPD
5, 12313–12371, 2005

More detailed boundary layer structure measurements in combination with back trajectory analysis during the NAMBLEX campaign is described by Norton et al. (2005). However, caution must be used when assigning air-mass sectors only according to local in-situ wind direction as measurements during the NAMBLEX data did not necessarily correspond with the origin of the air-mass back-trajectory analysis. For example, there were a number of land-sea breeze events (particularly at night). From 1 to 5 August, these breeze events brought local easterly winds to the site during westerly trajectories.

The British Atmospheric Data Centre's (BADC) trajectory service (http://www.badc.nerc.ac.uk) was used to plot five-day air-mass back-trajectories at six-hourly intervals. According to the origin of the air-masses of these trajectories, a new division into seven areas of origin was developed as shown in Tables 1, 2 and 3. The most common air-mass sector was the north-westerly (NW), followed by westerly (W) and then south-westerly (SW) as shown in Fig. 1a (see also Heard et al., 2005). Examples of three typical NW, W and north-easterly (NE) air-mass sector back-trajectories are shown in Fig. 1b. The effects of local sea and coastal breezes were removed from the analysis by only selecting data where the local wind speed was greater than $3\,m\,s^{-1}$ (Salisbury et al., 2002).

Table 1 shows the average $HO_2+\Sigma RO_2$, NO_x, CO, CH_4, O_3, CH_3OOH, H_2O_2, HCHO, DMS, isoprene, benzene and methanol mixing ratios and $j(O^1D)$ for the corresponding air-mass sectors. The data in Table 2 corresponds to the daylight (06:00–19:00) averages. Table 3 shows the night-time concentrations of the same species, as well as $[NO_3]$ and total alkenes.

3.2. Chemical climatology

Heard et al. (2005) provide a comprehensive overview of all the other species and supporting measurements made during NAMBLEX and their respective time series.

3.2.1. Peroxy radical levels and diurnal cycles

The data in Table 1 and the peroxy radical time series in Fig. 2 show that peroxy radical concentrations are highest when the air is of continental origin (S, E and NE air-mass sectors). Also the concentrations of NO_x, isoprene and formaldehyde were significantly higher in these sectors than in the marine W sector.

The lowest peroxy radical concentrations during the campaign were near the detection limit of the instrument (see experimental section) at around 1 pptv but were rarely less than 4 pptv, even at night. The maximum peroxy radical concentration reached 60 pptv for the occasional short-lived spike and 40 pptv for midday maximum values (see Fig. 2). Generally, the day-time peroxy radical concentrations were between two and three times higher than night-time levels.

The campaign average $[HO_2+\Sigma RO_2]$, $[NO_x]$ and $j(O^1D)$ diurnal cycles and the W and NE air-mass sector-averaged diurnal cycles are shown in Fig. 3. Peroxy radicals track the $j(O^1D)$ diurnal cycle fairly closely, with the cycle being shifted towards the end of the day as high midday concentrations persist well into the afternoon. This form of asymmetrical diurnal cycle has been noted before in low-NO_x environments by Monks et al. (1996) at Cape Grim, Carpenter et al. (1997) at Mace Head in 1995, and in high NO_x environments by Holland et al. (2003) and Mihelcic et al. (2003) at the BERLIOZ campaign near Berlin. In each of these environments there are different mechanisms that drive this asymmetry. The peroxy radical diurnal cycle for the W air-mass sector has less relative variability, tracking $j(O^1D)$ with a slight bias in maxima towards the afternoon. The NE sector peroxy radical diurnal is broader in both the morning and the evening. The S sector diurnal cycle (not shown) follows a similar pattern to the NE average in that it has a broader shape in both the morning and the afternoon.

An extensive modelling study by Sommariva et al. (2005a) has investigated the impact of oxygenate and halogen chemistry on the radical chemistry. Table 4 shows the sensitivity of the average model/measurement agreement for $HO_2+\Sigma RO_2$ with varying model assumptions. Figure 4a shows the results using the full oxygenate chemistry

ACPD
5, 12313–12371, 2005

constrained to measured IO with corrected heterogeneous uptake model and measured peroxy radical concentrations for the 15–22 August, and the same model run with the measured HO_2 from the FAGE instrument (Smith et al., 2005). For the model run with full oxygenate chemistry constrained to measured IO with corrected heterogeneous uptake (see Table 4), the peroxy radical measurement-model agreement is within the uncertainty of both the model and measurements. In general, the radical measurements are slightly higher than the model during the day-time. However, the model HO_2 constantly over-predicts the measured HO_2 concentrations, by at least a factor of 2–3 (Sommariva et al., 2005a). Inclusion of the halogen chemistry, in terms of measured IO seems to give some small improvement in the agreement. It is worth noting that there is some evidence for spatial inhomogeneity in the [IO] and the "local" [IO] could be a factor or 10 higher than that measured by long-path DOAS methods (see Sommariva et al., 2005a; Smith et al., 2005). The effect of halogens on the partitioning of NO and NO_2 and OH and HO_2 is dealt with later. Figure 4b shows a correlation plot of modelled PERCA peroxy radical (full+oxy, heterogeneous with IO chemistry, see Table 4) concentrations against measured values for all fifteen minute-averaged data and also the hourly-averages with their corresponding standard deviation. From Fig. 4b, there is a good correlation with the slope $=1.0_2$ (R^2=0.73). At low [$HO_2+\sum RO_2$], the model-measurement comparison lies below the 1:1 line. At higher [$HO_2+\sum RO_2$], there is a wider spread of data and the model, particularly for the hourly averages around solar noon over-predicts the measured peroxy radical levels.

$j(O^1D)$, $\sqrt{j(O^1D)}$ vs. [$HO_2+\Sigma RO_2$] correlations and diurnal cycles for the 23 and 24 August are shown in Fig. 5. The back trajectories shown in Fig. 5 suggest a SW air-mass origin on 23 August coming off the French coast, bringing higher concentrations of CO, CH_4, acetone, methanol and NO_x. The following day, the air-mass changes to a cleaner NW origin, where the NO/NO_x ratio and [NMHC] are significantly lower. The narrower shape of the diurnal cycle on 24 August could be due to a reduction in species that could be photolysed to form peroxy radicals.

On the NW day (24 August), peroxy radicals track $j(O^1D)$, whereas on the SW day

(23 August), the peroxy radicals have a broader shape than $j(O^1D)$. The correlation with both $j(O^1D)$ and $\sqrt{j(O^1D)}$ (r^2=0.87 and 0.89, respectively) is good on the NW day but poor (r^2=0.30 and 0.43) on the SW day. Since the correlation with $j(O^1D)$ on the SW day is poor, this is suggestive of an increased secondary source of HO_x from the photolysis of other compounds. This is particularly apparent in the early morning and the evening.

Photolysis of species other than O_3 (e.g. HCHO, HONO, H_2O_2, CH_3O_2H) could lead to a broadening of the peroxy radical diurnal cycle noted in the afternoon or early morning, when $j(O^1D)$ (primary production) is reduced. $[HO_2+\sum RO_2]$ vs. j(HCHO) correlations are divided into five different periods of the day in Fig. 5. On the 23 August, the largest increase in peroxy radicals as j(HCHO) increases was seen at 06:00–08:00 and 15:00–17:00. Despite the large increase in peroxy radicals with increasing j(HCHO) between 06:00 and 08:00, the j(HCHO) values were very low and would not have led to significant peroxy radical formation from this channel alone. Between 17:00–19:00 the product j(HCHO).[HCHO] was significantly large as to produce peroxy radicals at this time when $j(O^1D)$ was greatly reduced. The 24 August showed very poor trends. The same form of analysis with j(HONO) showed no observable trends (N.B. [HONO] estimated).

Figure 6a shows the campaign averaged [HCHO] and $[HO_2+\sum RO_2]$ diurnal cycles and the amount of HCHO photolysed each hour (j(HCHO).[HCHO]). Formaldehyde has a shifted diurnal cycle with values persisting into the evening. Daily maximum [HCHO] were around 1.6 ppbv (Still et al., 2005), much higher than the 0.2–0.8 ppbv found during a comparable campaign at Mace Head (Cardenas et al., 2000). The relative performance of the different HCHO measurement methods are discussed in Still et al. (2005).

Figure 6b shows correlation plots of $[HO_2+\sum RO_2]$ and [HCHO] against the amount of formaldehyde photolysed per hour (j(HCHO).[HCHO]). Both peroxy radicals and formaldeyde show a good correlation with formaldehyde photolysis. Formaldehyde is both a source of peroxy radicals (through photolysis and OH oxidation) and is pro-

ACPD
5, 12313–12371, 2005

duced from the peroxy radical reactions with NO. Figure 6b correlates peroxy radical and formaldehyde concentrations to the HO_2 production rate from formaldehyde photolysis. In the radical channel (14), one HCHO molecule yields two HO_2 molecules upon photolysis

$$\text{HCHO} + h\nu \rightarrow \text{H}_2 + \text{CO} \quad \text{(R13)}$$
$$\rightarrow \text{H} + \text{HCO} \quad \text{(R14)}$$

$$\text{H} + \text{O}_2 + \text{M} \rightarrow \text{HO}_2 + \text{M} \quad \text{(R8)}$$

$$\text{CHO} + \text{O}_2 \rightarrow \text{HO}_2 + \text{CO} \quad \text{(R15)}$$
$$\text{Overall : HCHO} + \text{O}_2 + h\nu \rightarrow 2\text{HO}_2 + \text{CO} \quad \text{(R16)}$$

The good correlation is suggestive of persistent peroxy radical levels in the late afternoon having a major contribution from formaldehyde photolysis.

An interesting phenomenon was observed on a number of days (namely the 9, 15, 17 and 31 August and 1 September); when the solar intensity and photolysis rates showed a sudden increase in the early evening and a disproportionately large peroxy radical increase was observed. On 21 August (see case day 21 August in Fig. 7a) a peak in the $j(O^1D)$ was accompanied by a sudden peroxy radical increase at around 17:00. The same increase in [OH] was observed by (Smith et al., 2005) on this day, and was reflected in the modelled [OH] (Sommariva et al., 2005a). The HO_2 measurements did not show a similar increase. One possible explanation for the phenomena is that if there are clouds at a given height as the sun nears the horizon light passes beneath the cloud at high zenith angles, rather than been attenuated by them, giving a short-lived boost to photochemical peroxy radical production (see for example, Monks et al., 2004).

ACPD
5, 12313–12371, 2005

3.3. Peroxy radicals and NO_x

NO_x concentrations of greater than 0.5 ppbv and up to as high as 2 ppbv were reached on 1–4 August and 8, 16 and 21 August (see Fig. 2). Between 1–4 August, air arrived from the E air-mass sector and the trajectories on the 8, 16 and 21 August were classified as W, despite some local polluted SE winds. $[NO_x]/[NO_y]$ were higher than average on the 13, 14 and 16 August (days where local pollution re-circulated at the site). All the case days (8 August, 16 August and 21 August) in Figs. 7a, b and c had very high $[NO_x]$ and a peroxy radical diurnal profile that is shifted towards the evening. This may be due to a suppression of peroxy radical formation when NO_x was high, and a sudden period of formation later in the day when NO_x levels dropped.

The campaign average $[NO_x]$ diurnal cycle is shown in Fig. 3. The values are highest between 09:00 and 12:00. High NO_x levels in the morning suppress via the repartitioning of HO_2 to OH. Peroxy radical concentrations and this NO_x suppression may, indeed, contribute to the apparent shift in the peroxy radical diurnal cycle. On the 16 August in Fig. 7b a sudden NO_x spike in the morning perturbed the peroxy radical concentrations, moving the apparent maximum towards the afternoon.

Peroxy radical concentrations vs. binned $[NO_x]$ (on a logarithmic scale) for all 10-min data are shown in Fig. 8a. The peroxy radicals were divided into three regimes according to $j(O^1D)$ values; $j(O^1D)>7.5\times10^{-6}\,s^{-1}$ represents daylight values, $3\times10^{-7}\,s^{-1}<(j(O^1D))<7.5\times10^{-6}\,s^{-1}$ represents dusk and dawn values or very cloudy conditions and $<3\times10^{-7}\,s^{-1}$ represents night-time conditions, which are discussed later.

The data with $j(O^1D)>7.5\times10^{-6}\,s^{-1}$ (daylight hours) are used for investigating the effect of NO_x on peroxy radicals during the day. Peroxy radical concentrations decrease with increasing $[NO_x]$ until values of about 0.1 ppbv $[NO_x]$. This shift is a result of changes in the HO_2:OH ratios towards OH (reactions of HO_2 and RO_2 with NO to form NO_2). Between values of 0.1 and 0.2 ppbv $[NO_x]$, there is a sudden increase in $[HO_2+\sum RO_2]$, which suggests a switch between NO_x- and VOC-limited conditions

ACPD
5, 12313–12371, 2005

with respect to ozone production. The corresponding increase in VOCs at [NO_x] above 0.1 ppbv would lead to a rise in OH oxidation of VOCs, producing more peroxy radicals. Above 0.2 ppbv [NO_x], increasing [NO_x] appears to lower [$HO_2 + \sum RO_2$].

Hourly averaged daylight (06:00–19:00) alkane, isoprene, HCHO, CO and CH_4 concentrations, as well as peroxy radical levels, are plotted against binned NO_x in Fig. 8b. The right-hand axis is scaled for each hydrocarbon. The sharp increase in all VOCs at [NO_x]>0.1 ppbv would have a strong link to the rise in peroxy radicals at this time. These high VOC levels change the reactive mixture with respect to peroxy radical speciation. Sudden NO_x increases could reflect changing air-mass composition. Concentrations of the biogenic hydrocarbon, isoprene peak at a lower [NO_x] than the corresponding anthropogenic hydrocarbons. At higher [NO_x], it is not clear which hydrocarbons govern the organic peroxy radical concentrations. Until 0.1 ppbv [NO_x], the peroxy radical trend with increasing [NO_x] is very similar to the HCHO trend. At [NO_x] between 0.5 and 1 ppbv the dependence of peroxy radicals on VOCs is very clear, as a drop in all VOCs is reflected in the peroxy radical data.

The rural marine boundary location of Mace Head was seen to be representative of background chemistry but polluted air masses regularly reach the site, bringing higher NO_x levels than experienced in the marine W air-masses as shown in Rickard et al. (2002). The switch to a significant VOC contribution to [$HO_2 + \sum RO_2$] occurs at a lower [NO_x] level than at more polluted continental urban locations, such as at the BERLIOZ campaign where the maximum [HO_2] was at 1 ppbv [NO_x] (Holland et al., 2003).

3.4. Hydrocarbons and $HO_2/(HO_2 + \sum RO_2)$ ratios

The highest mixing ratio of anthropogenic source compounds such as ethene, toluene and benzene was observed between 1 and 5 August. This illustrates the more polluted VOC-laden air masses, originating from the NE sector, passing over Scandinavia, northern Britain and Ireland, as shown in Fig. 1b.

High isoprene concentrations between 2 and 4 August were followed immediately

by a sharp increase in DMS and this was also seen on the 17 and 30 August. DMS concentrations varied from concentrations barely above the detection limit to as high as 900 pptv, with a spike of over 1.5 ppbv on 28 July. DMS levels were highest in the W, N and SW sectors, as shown in Table 1.

OH reacts with hydrocarbons, forming organic radicals, which rapidly react with O_2 to form peroxy radicals (see Reactions 10 and 11). Lewis et al., (2005) calculated the percentage contribution to OH removal by VOCs by combining all the VOC-OH reaction rates, k_{VOC}[VOC][OH]. Acetaldehyde accounted for up to 20%, CH_4, and formaldehyde both up to 30% and the other measured non-methane hydrocarbons (NMHCs) between 10 and 15% of OH loss.

HO_2 measurements taken by FAGE (Smith et al., 2005) provide a means of comparing HO_2 with $HO_2 + \sum RO_2$. Figure 9a shows the measured and modelled (full+oxy, heterogeneous with IO chemistry, see Table 4), hourly-averaged $HO_2/HO_2 + \sum RO_2$ ratios during the period 15–22 August. The addition of halogens to the system can repartition both OH and HO_2 and NO and NO_2 (e.g. Monks, 2005) via

$$XO + HO_2 \rightarrow HOX + O_2 \quad \text{(R17)}$$

$$HOX + h\nu \rightarrow X + OH \quad \text{(R18)}$$

and

$$XO + NO \rightarrow X + NO_2 \quad \text{(R19)}$$

The measured $HO_2/(HO_2 + \sum RO_2)$ ratios are lower when [NO_x] is low as on 18 and 19 August and can reach values over 1 when NO_x-laden air arrives at the site. The $HO_2/(HO_2 + \sum RO_2)$ ratio generally decreases from the start of the day towards sunset. The equivalent model ratio shows a similar diurnal profile from day to day, with the distinct diurnal profile displaying the highest $HO_2/HO_2 + \sum RO_2$ ratios at midday. Generally, the modelled $HO_2/HO_2 + \sum RO_2$ ratio is much higher than the measurement equivalent, except when NO_x is high.

The correlation plot of modelled versus measured $HO_2/(HO_2 + \sum RO_2)$ ratios is shown in Fig. 9b, with the individual days marked in separate colours. The model

generally over-predicts these ratios on all the days. The measured $HO_2/(HO_2+\sum RO_2)$ ratio on 16 August (when local SE winds brought high NO_x levels to the site) showed large variations throughout the day, both for the modelled and measured ratios as seen in both Figs. 9a and b. However, Fig. 9a shows that the measurement ratios displayed greater variability during the high NO_x period on this day. The same is observed during the high NO_x period on 21 August, where the model ratio appears not to be influenced by NO_x variations.

To investigate the effect of varying NO_x on the $HO_2/(HO_2+\sum RO_2)$ ratio, a plot of $HO_2/(HO_2+\sum RO_2)$ ratios against binned $[NO_x]$ is shown in Fig. 8c. The ratio of inorganic to organic peroxy radicals increases as $[NO_x]$ increases. The highest $[NO_x]$ bin at 1 ppbv has been divided into smaller bins in order to study the structure at high NO_x. At $[NO_x]>0.8$ ppbv, the $HO_2/(HO_2+\sum RO_2)$ ratio appears to decrease with increasing $[NO_x]$. RO_2 reacts rapidly with NO to form formaldehyde, and its subsequent breakdown can lead to HO_2 formation.

Figure 8d shows the measured and modelled $HO_2/(HO_2+\sum RO_2)$ ratios plotted against $[NO_x]$. Two model runs (with and without IO) are plotted to show the effect of halogens. In general, the $HO_2/(HO_2+\sum RO_2)$ ratio is higher in the model but the model does not show a strong increase with increasing $[NO_x]$. $HO_2/(HO_2+\sum RO_2)$ ratios at high $[NO_x]$ for both model and measured values are very similar, but at lower $[NO_x]$ the model predicts higher $HO_2/(HO_2+\sum RO_2)$ ratios. Interestingly, the addition of halogen chemistry improves the agreement between model and measurement, indicating a role for the IO in repartitioning the OH and HO_2 via Reactions (16) and (17). It is clear that at low $[NO_x]$ the halogens seem to be more important. Sommariva et al. (2005) found that the model mechanism worked better at high NO_x, indicating that peroxy-peroxy reactions at low NO_x are still not fully understood. An earlier Mace Head campaign tailored box model, without OVOC and halogen chemistry, used on Mace Head data, over-predicted $HO_2/(HO_2+RO_2)$ at low NO_x and under-predicted at high NO_x (Carslaw et al., 1999, 2002).

As previously stated, oxidation of CO, CH_4, HCHO and NMHCs represents a large

ACPD
5, 12313–12371, 2005

loss term for OH. The reaction of OH with CO and HCHO leads to the formation of HO_2. OH reaction with CH_4 forms CH_3O_2 and OH reaction with VOC forms predominantly RO_2. The fraction of OH removal reactions that form HO_2 can be represented as:

$$\phi(\mathrm{CO + HCHO}) = \left(\frac{k_{co}[\mathrm{CO}] + k_{\mathrm{HCHO}}[\mathrm{HCHO}]}{k_{co}[\mathrm{CO}] + k_{\mathrm{HCHO}}[\mathrm{HCHO}] + k_{\mathrm{CH_4}} + k_{\mathrm{voc}}[\mathrm{VOC}]} \right) [\mathrm{OH}] \quad (1)$$

where k_{CO}, k_{HCHO}, k_{CH_4} and k_{VOC} are the rate coefficients for the reaction of OH with CO, HCHO, CH_4 and VOCs, respectively. The rate-coefficients were taken from the National Institute of Standards and Technology (NIST) web site.

The ϕ(CO+HCHO) fraction was calculated for the days that had complete CO, CH_4 and VOC and HCHO concentrations, as in Lewis et al. (2005). Comparing ϕ(CO+HCHO) ratios with $HO_2/(HO_2+\sum RO_2)$ ratios should be indicative of whether $HO_2/(HO_2+\sum RO_2)$ ratio variations were caused primarily by varying HCHO, CO, CH_4 and VOC concentrations.

Figure 8e shows a plot of hourly $HO_2/(HO_2+\sum RO_2)$ and ϕ(CO+HCHO) ratios against binned [NO_x]. The trend for increasing $HO_2/(HO_2+\sum RO_2)$ with increasing [NO_x] is not replicated for ϕ(CO+HCHO), which does not appear effected by NO_x. $HO_2/(HO_2+\sum RO_2)$ ratios are always lower than ϕ(CO+HCHO) ratios (<0.5 for $HO_2/(HO_2+RO_2)$ and >0.5 for ϕ(CO+HCHO)). The ratio of k[HCHO]/(k[HCHO]+k[CO]) was found to remain constant at around 0.5, showing that HCHO and CO contribute equally to HO_2 formation. ϕ(CO+HCHO) ratios have a range of between 0.3 and 2.5 in NAMBLEX, much greater than the $HO_2/(HO_2+\sum RO_2)$ ratio range. The ϕ(CO+HCHO) ratios were usually much higher than $HO_2/(HO_2+\sum RO_2)$ ratios, which suggests that modelling the VOC-OH reactivity underestimates the resulting RO_2 concentrations with respect to HO_2. Also, calculating HO_2 to be directly correlated with CO and HCHO reactivity is not necessarily valid as HCHO is both photolysed and is oxidised by OH to form HO_2. HCHO is also formed from the reaction of CH_3O_2 with NO (Reactions 2 and 3).

The HCHO:CO ratio can be used as a tracer to distinguish different air masses and

differing times since the last major input from pollution. It is of interest because both tracers are primary pollutants, but formaldehyde is also produced in the troposphere by oxidation of CH_4 in the presence of NO_x. Subsequent photolysis of this formaldehyde then produces CO. In polluted high NO_x environments, HCHO production is more important than its photolysis and the HCHO:CO ratio increases. Figure 10 shows that both $[HO_2 + \sum RO_2]$ and $[O_3]$ increase with increasing HCHO/CO. If higher HCHO:CO ratios are a marker for polluted conditions, then this would be likely to lead to higher ozone levels. Higher peroxy radical levels at increased HCHO suggests that HCHO is more effective at producing peroxy radicals than CO. The ϕ(CO+HCHO) ratio presumes that HCHO and CO have equal HO_2 productivity, so any discrepancy between ϕ(CO+HCHO) and $HO_2/HO_2 + \sum RO_2$ may be due to the inaccuracy of predicting HO_2 from ϕ(CO+HCHO).

3.5. Peroxides

The highest H_2O_2 concentrations of up to 0.5 pptv were between 1 and 3 August when NO_x and hydrocarbon concentrations were high. Indeed, in Table 1, high NO_x and high VOC concentrations in the E sector have lead to the highest peroxide concentrations. Morgan (2004) found a maximum $[H_2O_2]$ of 1.1 ppbv with an average of 0.19 ppbv during NAMBLEX, much lower than the maximum of 7.1 and mean of 1.58 ppbv at Mace Head in June 1999 (Morgan and Jackson, 2002). In the clean marine boundary layer, such as Cape Grim, Tasmania, peroxy radicals are more likely to self-react to form peroxides than they are to react with NO and subsequently produce ozone (Ayers et al., 1997). Thus, high levels of peroxides would signify an ozone-destroying regime and a lower turnover rate of the various species that are part of the ozone-forming cycles.

Figure 8f shows [peroxide] versus $[NO_x]$ trends that are very similar in shape to peroxy radical – NO_x trends in Fig. 8a, illustrating the strong link between peroxy radicals and H_2O_2 concentrations. H_2O_2 concentrations are highest at around 0.1 ppbv NO_x and decrease slightly at higher NO_x but do not decrease to the same extent as peroxy

ACPD
5, 12313–12371, 2005

radical levels at high NO_x as shown in in Fig. 8a. CH_3O_2H is more influenced by NO_x than H_2O_2, as it is reduced to nearly zero values at high NO_x.

3.6. Night-time chemistry

Table 3 shows night-time averages for the different air mass sectors and the concomitant NO_3 measurements from data on fifteen nights (Saiz-Lopez et al., 2005; see also Bitter et al., 2005[5]). The E and NE air-mass sectors have the highest average O_3, NO_3 (with the E sector having [NO_3] of 11.7 pptv, compared to less than 6 pptv in all the other sectors) and total alkene concentrations as seen in Table 3. The highest night-time peroxy radical concentrations are observed in the SE and E sectors (c.f. Allan et al., 2000).

Sommariva et al. (2005b)[4] found that the model had a tendency to underestimate night time peroxy radical levels except on 31 August and 1 September. Closer agreement between the model and measurements was achieved when moving from a "clean" model with only CO and CH_4 to the full model with more complex hydrocarbons. Short-term NO_x spikes during the night are often matched with elevated peroxy radical concentrations as high as 10 pptv, or even 25 pptv in the polluted E period on the 2 and 3 August. On 16 August, when [NO_x] suddenly increased at about 20:00, a significant rise in [$HO_2+\sum RO_2$] followed closely, as shown in the case day in Fig. 7b. [$HO_2+\sum RO_2$] vs. [NO_x] for nights with NO_3 data are shown in Fig. 8a. As [NO_x] increases, [HO_2+RO_2] increases at [NO_x]>0.1 ppbv. This peroxy radical increase with NO_x is suggestive of NO_3 radicals (in equilibrium with NO_2) reacting with hydrocarbons to form peroxy radicals.

Figure 11a is a plot of average [$HO_2+\sum RO_2$] vs. [NO_3] (Saiz-Lopez et al., 2005)

[5]Bitter, M., Ball, S. M., Povey, I. M., Jones, R. L., Saiz-Lopez, A., and Plane, J. M. C.: Measurements of NO_3, N_2O_5, OIO, I_2, water vapour and aerosol optical depth by broadband cavity ringdown spectroscopy during the NAMBLEX campaign, Atmos. Chem. Phys. Discuss., in preparation, 2005.

ACPD
5, 12313–12371, 2005

for all the air-mass sectors. The [$HO_2 + \sum RO_2$] were separated into six [NO_3] bins and plotted on the same graph with error bars showing their standard deviation. The E sector, even though [NO_3] varies widely, always has higher [$HO_2 + \sum RO_2$] than the other sectors, irrespective of [NO_3]. Figure 11b shows the night-time profiles of [NO_3] and [$HO_2 + \sum RO_2$] for the entire marine (N, NW, SW and W combined) and continental (NE, E combined) air-mass sectors. The NO_3 concentration was always higher in the continental sector. The peroxy radical concentration was also always higher in the continental sector. There does not appear to be a significant peroxy radical pattern throughout the night.

Rate constants for the reaction of NO_3 with the measured alkenes were used to calculate the rate of the NO_3 loss and the O_3 reactions with alkenes (c.f. Salisbury et al., 2001). The flux of peroxy radicals formed from the alkene reactions from the NO_3 and O_3 channels were compared by correlating all night-time hours of the campaign as shown in Fig. 12a. At low peroxy radical-forming fluxes, the ozone-alkene reactions tended to dominate over the NO_3-alkene reactions. When NO_3 levels were high, the fluxes from NO_3-alkene reactions were far higher than the ozone-alkene fluxes. At NO_3-alkene fluxes above 5×10^4 molecules cm^{-3} s^{-1}, the ozone-alkene flux was always lower than the NO_3-alkene flux. Figure 12b shows the percentage contribution to peroxy radical formation from alkene night-time reactions. This varies strongly from night to night, with high NO_3 contributions on 18 and 25 August, receiving W and SW air-masses, respectively. For the nights for which full data is available the overall contribution of ozone-alkene chemistry to peroxy radical production was 59% compared to 41% for NO_3-alkene.

Peroxy radical levels were seen to decrease throughout the night in EASE 97 (Salisbury et al., 2001), with more polluted conditions experiencing less of a decrease throughout the night. Analysis to determine the percentage contribution of the ozone-alkene and NO_3 reactions to form peroxy radicals was carried out for EASE 97 (Salisbury et al., 2001). The contribution of both was found to vary between 30 and 70%, for each wind sector, but on the whole as with this study the ozone-alkene reaction

was the dominant production mechanism. Carslaw et al. (1997) found a positive correlation between $HO_2 + \sum RO_2$ and NO_3 at the Weybourne Atmospheric Observatory, while Mihelcic et al. (1993) found a negative correlation between peroxy radicals and NO_3 (presumably owing to highly variable reactive hydrocarbon fluxes) at Schauinsland. Any lack of correlation is not surprising, as NO_3 is both a source (Wayne et al., 1991) and a sink (Biggs et al., 1994) of peroxy radicals.

3.7. Photochemical production of ozone

Net photochemical ozone formation, $N(O_3)$ (or ozone tendency) was calculated for each hour of the campaign between 06:00 and 19:00, using Eq. (3) (for assumptions inherent in this form of calculation see Salisbury et al., 2002). The production term represents NO_2 formation and subsequent photolysis to form ozone (Reactions 1 to 4). k_p is the combined rate coefficient for the oxidation of NO to NO_2 by all peroxy radicals (Reactions 1 and 2). The loss term represents the reaction of ozone with OH and HO_2 and ozone photolysis (where f represents the fraction of $O(^1D)$ that reacts with H_2O to form OH).

$$N(O_3) = P(O_3) - L(O_3) \quad (2)$$

$$N(O_3) = k_p[NO][HO_2 + \Sigma RO_2] - \{f.j(O^1D) + k_{21}[OH] + k_6[HO_2]\}[O_3] \quad (3)$$

$$HO_2 + O_3 \rightarrow OH + 2O_2 \quad (R6)$$

$$OH + O_3 \rightarrow HO_2 + O_2 \quad (R20)$$

Figure 13a shows a time series of calculated ozone loss for all campaign daylight hours. The largest contribution to the calculated loss is that of ozone photolysis. The average ozone loss chemistry was calculated to be 64% from ozone photolysis, 8% from the $OH+O_3$ reaction and 24% from the HO_2+O_3 reaction. The contributions from the three

ACPD
5, 12313–12371, 2005

loss reactions vary from day to day, with total ozone loss varying between 0.1 and 0.7 ppbv h^{-1} at the solar maximum.

Figure 13b is a plot of net ozone production, $N(O_3)$ throughout the campaign with $[HO_2+\Sigma RO_2]$ and [NO] plotted on the right-hand axis. The ozone production term, $P(O_3)$ is dependent on [NO] and $[HO_2+\Sigma RO_2]$, the ratio of which varies greatly from day to day, showing an inverse relationship during the daylight hours. [NO] was more variable than $[HO_2+\Sigma RO_2]$ during NAMBLEX. Lower [NO] leads to a smaller $P(O_3)$ term, which means that ozone loss becomes nearly as great as ozone production, leading to a few hours and days where $N(O_3)$ was negative.

Figure 14 shows the hourly-averaged ozone loss and production rates for NAMBLEX. The loss term follows $j(O^1D)$, peaking at solar noon, and does not vary widely from day to day. However, ozone production values show a high degree of variation between days, with midday values varying from 0.1 to 2.5 ppbv h^{-1}. The shift of the maximum ozone loss term towards the afternoon results in the net ozone production being lower in the afternoon than the morning. The rise in $P(O_3)$ in the late afternoon caused by high peroxy radical levels leads to an increase in net ozone production at 16:00. This averaged diurnal cycle appears to show overall ozone production but the high $P(O_3)$ during the polluted E air-mass sector period of 1–5 August shifts the balance to positive $N(O_3)$, despite the many periods of net ozone destruction.

Figure 15 shows $N(O_3)$ for 8 August. This was a day where high $[NO_x]$ reduced peroxy radical levels and the elevated [NO] led to higher net ozone production than on the days preceding and following it. A high NO_x episode in the morning delayed peroxy radical production until around 14:00 (Fig. 7c) and produced high $P(O_3)$. At 13:00 $P(O_3)$ was low because $[NO_x]$ dropped away, and the peroxy radical levels had not yet recovered. The build-up of peroxy radical levels in the afternoon led to a boost in $P(O_3)$ and another boost between 17:00 and 18:00 when night-time peroxy radical-forming reactions become important.

Figure 16 shows $N(O_3)$ plotted against $[NO_x]$. $N(O_3)$ rises sharply with increasing $[NO_x]$ until around 1 ppbv $[NO_x]$, when the increase in $N(O_3)$ levels off. The increase in

ACPD
5, 12313–12371, 2005

$N(O_3)$, with increasing NO_x, during the SOAPEX 2 campaign at Cape Grim, Tasmania showed very similar characteristics until $[NO_x]$ of 0.5 ppbv. Investigations of the effect of NO_x on $N(O_3)$ at Mace Head during the spring campaign of EASE 97 showed a much steeper increase in $N(O_3)$ at similar NO_x levels to those seen during NAMBLEX. Table 5 shows the ozone production values for Mace Head – EASE 97 (Salisbury et al., 2002), Cape Grim – SOAPEX 2 (Monks et al., 2005) and NAMBLEX, demonstrating the much higher range during the spring EASE 97 campaign.

Mace Head has experienced a positive trend in background ozone of 0.49 ± 0.19 ppb year^{-1} since 1987 (Simmonds et al., 2004), the largest trend being during the winter season. The behaviour of this trend may be attributed to the sensitivity of the background ozone level to changing European emissions of NO_x and VOC (Derwent et al., 2003; Monks, 2003). Following the methodology of Stroud et al. (2004) the sensitivity of $P(O_3)$ to NO was calculated as $d\ln P(O_3)/d\ln(NO)$, as shown in Fig. 17, for a series of marine boundary layer campaigns with differing continental influences. Table 6 summarises the derived sensitivity values of the ozone production term to NO. Both the Mace Head data sets have ozone production with linear sensitivity (i.e. $d\ln P(O_3)/d\ln(NO)=1$) to NO as compared to Cape Grim and Weybourne, that have values of around 0.9. The Mace Head values imply that the ozone production rate is strongly dependent on the [NO]. The equivalent derived values of $d\ln L(O_3)/d\ln(NO)$ are also given in Table 6 the bulk of these values range from ca. 0 to 0.3, unsurprisingly this suggests that $L(O_3)$ is generally independent of small changes in [NO]. In tandem, these results imply that the $N(O_3)$ will be strongly sensitive in the marine boundary layer to small changes in [NO].

4. Conclusions

During NAMBLEX, the Mace Head Atmospheric Research Station received a substantial mix of air-masses from both the Atlantic and from Britain and Ireland. 80% of the air-masses were from the clean N, NW, W and SW sectors. The marine air-mass sec-

ACPD
5, 12313–12371, 2005

tors had peroxy radical levels below 10 pptv, whereas the other sectors experienced levels above 13 pptv. The higher peroxy radical concentrations in the air-mass sectors with a continental influence were accompanied by over twice as high NO_x levels and much higher anthropogenic hydrocarbon mixing ratios.

Peroxy radical diurnal cycle maxima were typically shifted towards the afternoon, with daily maximum levels between 10 and 40 pptv. MCM modelling of peroxy radical levels provided a good model-measurement comparison, with occasional slight over-estimations by the box model.

Correlations of peroxy radicals with $j(O^1D)$ were often disturbed by NO_x episodes that temporarily lowered peroxy radical levels. No significant reliable linear or square root dependence with $j(O^1D)$ was observed to make a clear separation between clean and polluted conditions. Photolysis of compounds other than ozone led to a broader peroxy radical diurnal cycle than would be seen from production via ozone photolysis alone, especially in continentally-influenced air-masses. Correlations with $j(HCHO)$ in the afternoon and a definite shift in the HCHO diurnal cycle towards the afternoon suggests the high potential for HCHO photolysis at this time. A sudden increase in photolysis rates (i.e. a rise in $j(O^1D)$) in the early evening was seen to cause a large pulse in peroxy radicals.

Short-term large NO_x mixing ratios, termed "NO_x spikes", reaching the site caused a marked drop in peroxy radical levels. Plotting the overall effect of NO_x on peroxy radical levels during the whole campaign demonstrated a decrease in peroxy radicals with increasing NO_x. A break in the linear decrease around 0.1 and 0.2 ppbv NO_x was accompanied by an increase in VOCs which led to a short period where peroxy radicals actually increased with NO_x. This VOC influence on peroxy radicals could be thought of as the break between NO_x- and VOC-limited ozone producing regimes.

Comparisons with FAGE HO_2 measurements have shown that $HO_2/(HO_2+\sum RO_2)$ ratios are dependent on $[NO_x]$ and ranged between 0.2 and 0.6. $HO_2/(HO_2+\sum RO_2)$ ratios increase remarkably linearly with increasing NO_x. The MCM model did not replicate this NO_x-dependence with the model in general over-estimating

ACPD
5, 12313–12371, 2005

$HO_2/(HO_2+\sum RO_2)$ ratios. The addition of halogen oxide chemistry improved the level of agreement. Calculating the expected $HO_2/(HO_2+\sum RO_2)$ ratios from OH oxidation reactions of VOC, HCHO and CO did not show any significant NO_x-dependence.

Night-time peroxy radical concentrations rose to as high as 25 pptv in continental air-masses with high NO_x. Sudden NO_3 spikes definitely caused an increase in peroxy radicals, but constant higher NO_3 levels did not necessarily lead to higher peroxy radical concentrations. Peroxy radical and NO_3 mixing ratios were higher in continental compared to marine air-masses. The contribution of ozone-alkene and NO_3-alkene reactions to peroxy radical formation varies from night to night and there are variations as to which one predominates. At low NO_3, ozone-alkene reactions are always predominant.

Net photochemical ozone production reached as high as 1.5 ppbv h^{-1} with the lowest values being negative at -0.5 ppbv h^{-1}. Highest net ozone production was observed during high NO_x periods, demonstrating a clear increase in ozone production at higher NO_x. The ozone production rate is strongly dependent on [NO] having a linear sensitivity ($d\ln(P(O_3))/d\ln(NO)=1.0$). The results imply that the $N(O_3)$ will be strongly sensitive in the marine boundary layer to small changes in [NO] which has ramifications for changing NO_x loadings in the European continental boundary layer.

Acknowledgements. This work was conducted under the auspices of the UK-NERC funded project NAMBLEX. The authors would like to thank G. Spain for his logistical support, and also G. Johnson for assistance with HO_2 measurements using FAGE.

References

Allan, B. J., Carslaw, N., Coe, H., Burgess, R. A., and Plane, J. M. C.: Observations of the nitrate radical in the marine boundary layer, J. Atmos. Chem, 33, 129–154, 1999.

Allan, B. J., McFiggans, G., Plane, J. M. C., Coe, H., and McFadyen, G. G.: The nitrate radical in the marine boundary layer, J. Geophys. Res., 105, 24 191–24 204, 2000.

Andrés Hernández, M. D., Burkert, A. J., Reichert, L., Stöbener, D., Meyer-Arnek, J., Burrows, J. P., Dickerson, R. R., and Doddridge, B. G.: Marine boundary layer peroxy radical chemistry

during the AEROSOLS99 campaign: Measurements and analysis, J. Geophys. Res., 106, 20 833–20 846, 2001.

Ashbourn, S. F. M., Jenkin, M. E., and Clemitshaw, K. C.: Laboratory studies of the response of a peroxy radical chemical amplifier to HO_2 and a series of organic peroxy radicals, J. Atmos. Chem., 29, 233–266, 1998.

Ayers, G. P., Penkett, S. A., Gillett, R. W., Bandy, B. J., Galbally, I. E., Meyer, C. P., Elsworth, C. M., Bentley, S. T., and Forgan, B. W.: Evidence for photochemical control of ozone concentrations in unpolluted air, Nature, 360, 446–448, 1992.

Ayers, G. P., Granek, H., and Boers, R: Ozone in the Marine Boundary Layer at Cape Grim: Model Simulation, J. Atmos. Chem, 27, 179–195, 1997.

Ayers, G. P., Gillet, R. W., Granek, H., de Serves, C., and Cox, R. A: Formaldehyde production in clean marine air, Geophys. Res. Lett., 24, 401–404, 1997.

Biggs, P., Canosa-Mas, C. E., Fracheboud, J.-M., Shallcross, D. E., and Wayne, R. P.: Investigation into the kinetics and mechanism of the reaction of NO_3 with CH_3O_2 at 298 K and 2.5 Torr: A potential source of OH in the nighttime troposphere?, J. Chem. Soc. Faraday Trans, 90, 1205–1210, 1994.

Bloss, C., Wagner, V., Bonzanini, A., Jenkin, M. E., Wirtz, K., Martin-Reviejo, M., and Pilling, M. J.: Evaluation of detailed aromatic mechanisms (MCMv3 and MCMv3.1) against environmental chamber data., Atmos. Chem. Phys., 5, 623–639, 2005a, SRef-ID: 1680-7324/acp/2005-5-623.

Bloss, C., Wagner, V., Jenkin, M. E., Volkamer, R., Bloss, W. J., Lee, J. D., Heard, D. E., Wirtz, K., Martin-Reviejo, M., Rea, G., Wenger, J. C., and Pilling, M. J.: Development of a detailed chemical mechanism (MCMv3.1) for the atmospheric oxidation of aromatic hydrocarbons, Atmos. Chem. Phys., 5, 641–664, 2005b, SRef-ID: 1680-7324/acp/2005-5-641.

Bloss, W. J., Gravestock, T. J., Heard, D. E., Ingham, T., Johnson, G. P., and Lee, J. D.: Application of a compact all solid-state laser system to the in-situ detection of atmospheric OH, HO_2, NO and IO by laser-induced fluorescence, J. Environ. Monit., 5, 21–28, doi:10.1039/b208714f, 2003.

Bloss, W. J., Lee, J. D., Bloss, C., Wirtz, K., Martin-Reviejo, M., Siese, M., Heard, D. E., and Pilling, M. J.: Validation of the calibration of a laser-induced fluorescence instrument for the measurement of OH radicals in the atmosphere, Atmos. Chem. Phys., 4, 571–583, 2004, SRef-ID: 1680-7324/acp/2004-4-571.

Bloss, W. J., Lee, J. D., Johnson, G. P., Sommariva, R., Heard, D. E., Saiz-Lopez, A., Plane, J. M. C., McFiggans, G., Coe, H., Flynn, M., Williams, P., Rickard, A. R., and Fleming, Z. L.: Impact of halogen monoxide chemistry upon boundary layer OH and HO_2 concentrations at a coastal site, Geophys. Res. Lett., 32, L06814, doi:10.1029/2004GL022084, 2005c.

Brough, N., Reeves, C. E., Penkett, S. A., Dewey, K., Barjat, H., Monks, P. S., Ziereis, H., Stock, P., Huntrieser, H., and Sclager, H.: Intercomparison of aircraft instruments on board the C-130 and Falcon 20 over Southern Germany during EXPORT 2000, Atmos. Chem. Phys., 3, 2127–2138, 2003,
SRef-ID: 1680-7324/acp/2003-3-2127.

Cantrell, C. A., Stedman, D. H., and Wendel, G. J.: Measurement of atmospheric peroxy radicals by chemical amplification, Anal. Chem., 56, 1496–1502, 1984.

Cantrell, C. A., Shetter, R. E., Gilpin, T. M., Calvert, J. G., Eisele, F. L., and Tanner, D. J.: Peroxy radical concentrations measured and calculated from trace-gas measurements in the Mauna Loa Observatory Photochemistry Experiment 2, J. Geophys. Res., 101, 14 653–14 644, 1996a.

Cantrell, C. A., Shetter, R. E., and Calvert, J. G.: Dual-inlet Chemical amplifier for atmospheric peroxy radical measurements, Anal. Chem., 58, 4194–4199, 1996b.

Cantrell, C. A., Shetter, R. E., Calvert, J. G., Eisele F. L., Williams, E., Baumann, K., Brune, W. H., Stevens, P. S., and Mather, J. H.: Peroxy radicals from photostationary-state deviations and steady-state calculations during the Tropospheric OH Photochemistry Experiment at Idaho Hill, Colorado, 1993, J. Geophys. Res., 102, 6369–6378, 1997

Cardenas, L. M., Brassington, D. J., Allan, B. J., Coe, H., Alicke, B., Platt, U., Wilson, K. M., Plane, J. M. C., and Penkett, S. A.: Intercomparison of formaldehyde measurements in clean and polluted atmospheres, J. Atmos. Chem., 37, 53–80, 2000.

Carpenter, L. J., Monks, P. S., Bandy, B. J., and Penkett, S. A.: A study of peroxy radicals and ozone photochemistry at coastal sites in the northern and southern hemispheres, J. Geophys. Res., 102, 25 417–25 427, 1997.

Carslaw, N., Carpenter, L. J., Plane, J. M. C., Allan, B. J., Burgess, R. A., Clemitshaw, K. C., Coe, H., and Penkett, S. A.: Simultaneous observations of nitrate and peroxy radicals in the marine boundary layer,1. Model construction and comparison with field measurements, J. Geophys. Res., 102, 18 917–18 933, 1997.

Carslaw, N., Creasey, D. J., Heard, D. E., Lewis, A. C., McQuaid, J. B., Pilling, M. J., Monks, P. S., Bandy, B. J., and Penkett, S. A.: Modelling OH, HO_2 and RO_2 radicals in the marine

boundary layer 1. Model construction and comparison with field measurements, J. Geophys. Res., 104, 30 241–30 255, 1999.
Carslaw, N., Creasey, D. J., Heard, D. E., Jacobs, P. J., Lee, J. D., Lewis, A. C., McQuaid, J. B., Pilling, M. J., Bauguitte, S., Penkett, S. A., Monks, P. S., and Salisbury, G.: Eastern Atlantic Spring Experiment 1997 (EASE97) – 2. Comparisons of model concentrations of OH, HO_2, and RO_2 with measurements, J. Geophys. Res., 107, 4190, 2002.
Carslaw, N., Bell, N., Lewis, J. B., McQuaid, J. B., and Pilling, M. J.: A detailed study of isoprene chemistry during the EASE 96 campaign, Atmos. Environ., 34, 2827–2836, 2000.
Clemitshaw, K. C., Carpenter, L. J., Penkett, S. A., and Jenkin, M. E.: A calibrated peroxy radical chemical amplifier (PERCA) for ground-based measurements in the troposphere, J. Geophys. Res., 102, 25 405–25 416, 1997.
Creasey, D. J., Halford-Maw, P. A., Heard, D. E., Pilling, M. J., and Whitaker, B. J.: Implementation and initial deployment of a field instrument for measurement of OH and HO_2 in the troposphere by laser-induced fluorescence, J. Chem. Soc., Faraday Trans., 93(16), 2907–2913, 1997.
Creasey, D. J., Heard, D. E., and Lee, J. D.: The Eastern Atlantic Spring Experiment (EASE) 1997: (1) OH and HO_2 radical measurements at Mace Head, Eire, J. Geophys. Res., 107(D10), 892, 2002.
Creasey, D. J., Evans, G. E., Heard, D. E., and Lee, J. D.: Measurements of OH and HO_2 concentrations in the Southern Ocean marine boundary layer, J. Geophys. Res., 108, doi:10.1029/2002JD003206, 2003.
Derwent, R. G., Simmonds, P. G., and Collins, W. J.: Ozone and carbon monoxide measurements at a remote maritime location, Mace Head, Ireland from 1990 to 1992, Atmos. Environ., 28, 2623–2637, 1994.
Derwent, R. G., Simmonds, P. G., Seuring, S., and Dimmer, C: Observation and interpretation of the seasonal cycles in the surface concentrations of ozone and carbon monoxide at Mace Head, Ireland from 1990 to 1994, Atmos. Environ., 32, 145–157, 1998.
Derwent, R. G., Jenkin, M. E., Saunders, S. M., Pilling, M. J., Simmonds, P. G., Passant, N. R., Dollard, G. J., Dumitrean, P., and Kent, A.: Photochemical ozone formation in north west Europe and its control, Atmos. Environ., 37, 1983–1991, 2003.
Edwards, G. D. and Monks, P. S.: Performance of a single monochromator diode array spectrradiometer for the determination of actinic flux and atmospheric frequencies, J. Geophys. Res., 108, 8546–8558, 2003.

Fleming, Z. L.: The measurement of peroxy radicals in the marine boundary layer using the PERCA technique, Ph.D. Thesis, University of Leicester, 2005a.

Green, T. J., Brough, N., Reeves, C. E., Edwards, G. D., Monks, P. S., and Penkett, S. A.: Airborne measurements of peroxy radicals using the PERCA technique, J. Environ. Monitoring, 5, 75–83, 2003.

Grossman, D., Moortgat, G. K., Kibler, M., Schlomski, S., Bächmann, K., Alicke, B., Geyer, A., Platt, U., Hammer, M.-U., Vogel, B., Mihelcic, D., Hofzumahaus, A., Holland, F., and Volz-Thomas, A.: Hydrogen peroxide, organic peroxides, carbonyl compounds and organic acids measured at Pabstthum during BERLIOZ, J. Geophys. Res., 108, 8250, doi:10.1029/2001JD001096, 2003.

Heard, D. E., Read, K. A., Al-Haider, S., Bloss, W. J., Johnson, G. P., Pilling, M. J., Rickard A. R., Seakins, P. W., Smith, S. C., Sommariva, R., Stanton, J. C., Still, T., Brooks, B., Jackson, A. V., McQuaid, J. B., Morgan, R., Smith, M. H., Carslaw, N., Hamilton, J., Hopkins, J. R., Lee, J. D., Lewis, A. C., Purvis, R. M., Wevill, D. J., Brough, N., Green, T., Mills, G., Penkett, S. A., Plane, J. M. C., Saiz-Lopez, A., Worton, D., Monks, P. S., Fleming, Z., Alfarra, M., Allan, J. D., Bower, K., Coe, H., Cubison, M., Flynn, M., McFiggans, G., Gallagher, M., Norton, E. G., Shillito, J., Topping, D., Vaughan, G., Williams, P., Bitter. M., Ball, S. M., Jones, R. L., Povey, I. M., O'Doherty, S., Noone, C., Simmonds, P. G., Allen, A., Kinnersley, R., Beddows, D., Dall'Osto, M., Harrison, R. M., Donovan, R., Heal, M., Methven, J., Jennings, G., and Spain, G.: The North Atlantic Marine Boundary Layer Experiment (NAMBLEX). Overview of the campaign held at Mace Head, Ireland, in summer 2002, Atmos. Chem. Phys. Discuss., 5, 12 177–12 254, 2005,
SRef-ID: 1680-7375/acpd/2005-5-12177.

Heikes, B., Lee, M., Jacob, D., Talbot, R., Bradshaw, J., Singh, H., Blake, D., Anderson, B., Fuelberg, H., and Thompson, A.: Ozone, hydroperoxides, oxides of nitrogen, and hydrocarbon budgets in the marine boundary layer over the South Atlantic, J. Geophys. Res., 101, 24 221–24 234, 1996.

Holland, F., Hofzumahaus, A., Schäfer, J., Kraus, A., and Pätz, H.-W.: Measurements of OH and HO_2 radical concentrations and photolysis frequencies during BERLIOZ, J. Geophys. Res., 108, 8246–8267, 2003.

Hopkins, J. R., Lewis, A. C., Read, K. A.: A Two Column Method for Long-term Monitoring of Non-Methane Hydrocarbons (NMHCs) and Oxygenated Volatile Organic Compounds, J. Environ. Monit., 5, 8–13, 2003a.

Hopkins, J. R., Still, T., Al-Haider, S., Fisher, I. R., Lewis, A. C., and Seakins, P. W.: A simplified apparatus for ambient formaldehyde detection via GC-PHID, Atmos. Environ., 37, 2557–2565, 2003b.

Jenkin, M. E., Saunders, S. M., and Pilling, M. J.: The tropospheric degradation of volatile organic compounds: A protocol for mechanism development, Atmos. Environ., 31, 81–104, 1997.

Jenkin M. E, Saunders, S. M., Wagner, V., and Pilling, M.: Protocol for the development of the Master Chemical Mechanism, MCM v3 (Part A): tropospheric degradation of non-aromatic volatile organic compounds (Part B): tropospheric degradation of aromatic volatile organic compounds, Atmos. Chem. Phys., 3, 161–193, 2003, SRef-ID: 1680-7324/acp/2003-3-161.

Hu, J. and Stedman, D. H.: Atmospheric RO_x radicals at an urban site; Comparison to a simple theoretical model, Environ. Sci. Technol., 29, 1655–1659, 1995.

Hunter, M. C., Bartle, K. D., Seakins, P. W., and Lewis, A. C.: Direct measurement of atmospheric formaldehyde using gas chromatography-pulsed discharge ionisation detection, Anal Commun., 36, 101–104, 1999.

Kanaya, Y., Matsumoto, J., and Akimoto, H.: Photochemical ozone production at a subtropical island of Okinawa, Japan: Implications from simultaneous observations of HO_2 radical and NOx, J. Geophys. Res., 107, 4368, 2002.

Kotchenruther, R. A., Jaffe, D. A., and Jaeglé, L.: Ozone photochemistry and the role of peroxyacetlynitrate in the springtime Pacific troposphere: Results from the Photochemical Ozone Budget of the Eastern North Pacific Atmosphere (PHOBEA) campaign, J. Geophys. Res., 106, 28 731–28 742, 2001.

Kraus, A. and Hofzumahaus, A.: Field measurements of atmospheric photolysis frequencies for O_3, NO_2, HCHO, CH_3CHO, H_2O_2 and HONO by UV spectroradiometry, J. Atmos. Chem., 31, 161–180, 1998.

Lawson, D. R., Bierman, H. W., Tuazon, E. C., Winer, A. M., Mackay, G. I., Schiff, H. I., Kok, G. L., Dasgupta, P. K., and Fung, K.: Formaldehyde measurements methods evaluation and ambient concentrations during the carbonaceous species comparison study, Aerosol Sci. Technol., 12, 64–76, 1990.

Lewis, A. C., Bartle, K. D., McQuaid, J. B., Pilling, M. J., Seakins, P. W., and Ridgeon, P.: Atmospheric monitoring of volatile organic compounds using programmed temperature vaporisation injection, J. High Res. Chromat., 19, 686–690, 1996.

Lewis, A. C, Hopkins, J. R, Read, K. A., Carpenter, L. J., Pilling, M. J., and Stanton, J.: Sources and sinks of acetaldehyde, acetone and methanol in north Atlantic marine boundary layer air, Atmos. Chem. Phys., 5, 1963–1974, 2005, SRef-ID: 1680-7324/acp/2005-5-1963.

Mather, J. H., Stevens, P. S., and Brune, W. H.: OH and HO_2 measurements using laser-induced fluorescence, J. Geophys. Res., 102(D5), 6427–6436, doi:10.1029/96JD01702, 1997.

Metcalfe, S. E., Whyatt, J. D., Derwent, R. G., and O'Donoghue, M.: The regional distribution of ozone across the British Isles and its response to control strategies, Atmos. Environ., 36, 4045–4055, 2002.

Mihelcic, D., Klemp, D., Müsgen. P., Pätz, H. W., Kley, D., and Volz-Thomas, A.: Simultaneous measurements of peroxy and nitrate radicals at Schauinsland, J. Atmos. Chem., 16, 313–335, 1993.

Mihelcic, D., Holland, F., Hofzumahaus, A., Hoppe, L., Konrad, S., Müsgen, P., Pätz, H.-W., Schäfer, H.-J., Schmitz, T., Volz-Thomas, A., Bächmann, K., Schlonski, S., Platt, U., Geyer, A., Alicke, B., and Moorgat, G. K.: Peroxy radicals during BERLIOZ at Pabstthum: Measurements, radical budgets and ozone production, J. Geophys. Res., 108, 8254–8268, 2003.

Mihele, C. M. and Hastie, D. R.: The sensitivity of the radical amplifier to ambient water vapour, Geophys. Res. Lett., 25, 1911–1913, 1998.

Mihele, C. M., Mozurkewich, M., and Hastie, D. R.: Radical loss in a chain reaction of CO and NO in the presence of water: Implications for the radical amplifier and atmospheric chemistry, Int. J. Chem. Kin., 31, 145–152, 1999.

Monks, P. S., Carpenter, L. J., Penkett, S. A., Night-time peroxy radical chemistry in the remote marine boundary layer over the Southern ocean, Geophys. Res. Lett., 23, 535–538, 1996.

Monks, P. S., Carpenter, L. J., Penkett, S. A., Ayers, G. P., Gillett, R. W., Galbally, I. E., and Meyer, C. P.: Fundamental ozone photochemistry in the remote boundary layer: The SOAPEX experiment, measurement and theory, Atmos. Environ., 32, 3647–3664, 1998.

Monks, P. S., Holland, G. Salisbury, G. Penkett, S. A., and Ayers, G. P.: A seasonal comparison of ozone photochemistry in the remote marine boundary layer, Atmos. Environ., 34, 2547–2561, 2000.

Monks, P. S.: Tropospheric photochemistry, in: "Handbook of Atmospheric Science: Principle and Application", Chapter 6, edited by: Hewitt, C. N. and Jackson, A. V., Blackwell Publishing, Oxford, 2003.

Monks, P. S.: TROTREP Synthesis and Integration Report, Report to the EU FPV Energy, Environment and Sustainable Development Program, European Union, 2003.
Monks, P. S., Rickard, A. R., and Hall, S. L.: Attenuation of spectral actinic flux and photolysis frequencies at the surface through homogeneous cloud fields, J. Geophys. Res., 109, D17206, doi:10.1029/2003JD004076, 2004.
Monks, P. S.: Gas-phase radical chemistry in the troposphere, Chem. Soc. Rev., 34, 376–395, 2005.
Morgan, R. B. and Jackson, A. V.: Measurements of gas-phase hydrogen peroxide and methyl hydroperoxide in the coastal environment during the PARFORCE project, J. Geophys. Res, 107(D19), 8109, doi:10.1029/2000JD000257, 2002.
Morgan, R. B.: Field studies of atmospheric peroxides and the development of sampling methods, Ph.D. Thesis, University of Leeds, 2004.
Norton, E. G., Vaughan, G., Methven, J., Coe, H., Brooks, B., Gallagher, M., Longley, I.: Boundary layer structure and decoupling from synoptic scale flow during NAMBLEX, Atmos. Chem. Phys. Discuss., 5, 3191–3223, 2005, SRef-ID: 1680-7375/acpd/2005-5-3191.
Penkett, S. A., Blake, N. J., Lightman, P., Marsh, A. R. W., Anwyl, P., and Butcher, G.: The seasonal variation of non-methane hydrocarbons in the free troposphere over the North Atlantic Ocean: possible evidence for extensive reaction of hydrocarbons with the nitrate radical, J. Geophys. Res., 98, 2865–2885, 1993.
Penkett, S. A., Monks, P. S., Carpenter, L. J., and Clemitshaw, K. C.: Relationships between ozone photolysis rates and peroxy radical concentrations in clean air over the Southern Ocean, J. Geophys. Res., 102, 12 805–12 817, 1997.
Penkett, S. A., Clemitshaw, K. C., Savage, N. H., Burgess, R. A., Cardenas, L. M., Carpenter, L. J., McFadyden, G. G., and Cape, J. N.: Studies of oxidant production at the Weybourne Atmospheric observatory in summer and winter conditions, J. Atmos. Chem., 33, 111–128, 1999.
Platt, U., LeBras, G., Poulet, G., Burrows, J. P., and Moorgat, G.: Peroxy radicals from nighttime reaction of NO_3 with organic compounds, Nature, 348, 147–149, 1990.
Reichert, L., Hernandez, M. D. A., Stobener, D., Burkert, J., Burrows, J. P.: Investigation of the effect of water complexes in the determination of peroxy radical ambient concentrations: Implications for the atmosphere, J. Geophys. Res., 108, 4017, 2003.
Rickard, A. R., Johnson, D., McGill, C. D., and Marston, G.: OH yields in the gas-phase reac-

tions of ozone with alkenes, J. Phys. Chem., 103, 7656–7664, 1999.
Rickard, A. R., Salisbury, G., Monks, P. S., Lewis, A. C., Bauguitte, S., Bandy, B. J., Clemitshaw, K. C., and Penkett, S. A.: Comparison of measured ozone production efficiencies in the marine boundary layer at two European coastal sites under different pollution regimes, J. Atmos. Chem., 43, 107–134, 2002
Saiz-Lopez, A., Shillito, J. A., Coe, H., and Plane, J. M. C.: Measurements and modelling of I_2, IO, OIO, BrO and NO_3 in the mid-latitude marine boundary layer, Atmos. Chem. Phys. Discuss., 5, 9731–9767, 2005, SRef-ID: 1680-7375/acpd/2005-5-9731.
Salisbury, G., Rickard, A. R., Monks, P. S., Allan, B. J., Bauguitte, S., Penkett, S. A., Carslaw, N., Lewis, A. C., Creasy, D. J., Heard, D. E., Jacobs, P. J., and Lee, J. D.: Production of peroxy radicals at night via reactions of ozone and the nitrate radical in the marine boundary layer, J.Geophys.Res., 106, 12 669–12 687, 2001.
Salisbury, G., Monks, P. S., Bauguitte, S. Bandy, B. J., and Penkett, S. A.: A seasonal comparison of the ozone photochemistry in clean and polluted air masses at Mace Head, Ireland, J. Atmos. Chem., 41, 163–187, 2002.
Saunders, S. M., Jenkin, M. E., Derwen, R. G., and Pilling, M. J.: Protocol for the development of the Master Chemical Mechanism, MCM v3 (Part A): tropospheric degradation of non-aromatic volatile organic compounds, Atmos. Chem. Phys., 3, 161–180, 2003, SRef-ID: 1680-7324/acp/2003-3-161.
Sillman, S.: The use of NO_y, H_2O_2 and HNO_3 as indicators for ozone-hydrocarbon sensitivity in urban locations, J. Geophys. Res., 100(D7), 14 175–14 188, 1995.
Simmonds, P. G., Derwent R. G., Manning A. L., and Spain G.: Significant growth in surface ozone at Mace Head, Ireland, 1987–2003, Atmos. Environ., 38, 4679–4778, 2004.
Smith, S, Lee, J. D., Bloss, W. J., Johnson, G. P., Ingham, T., and Heard, D. E.: Concentrations of OH and HO_2 radicals during NAMBLEX: Measurement and steady-state analysis, Atmos. Chem. Phys. Discuss., in press, 2005.
Sommariva, R. C.: Understanding field measurements through a Master Chemical Mechanism, PhD thesis, University of Leeds, 2005.
Sommariva, R. , Bloss, W. J., Brough, N., Carslaw, N., Flynn, M., Haggerstone, A. -L., Heard, D. E., Hopkins, J. R., Lee, J. D., Lewis, A. C., McFiggans, G., Monks, P. S., Penkett, S. A., Pilling, M. J., Plane, J. M. C., Read, K. A., Saiz-Lopez, A., Rickard, A. R., and Williams, P. I.: OH and HO2 chemistry during NAMBLEX: roles of oxygenates, halogen oxides and

heterogeneous uptake, Atmos. Chem. Phys. Discuss., 5, 10 947–10 996, 2005a, SRef-ID: 1680-7375/acpd/2005-5-10947.

Still, T. J., Al-Haider, S., Seakins, P. W., Sommariva, R., Stanton, J. C., Mills, G., and Penkett S. A.: Ambient formaldehyde measurements made at a remote marine boundary layer site during the NAMBLEX campaign – a comparison of data from chromatographic and modified Hantzsch techniques, Atmos. Chem. Phys. Discuss, in press, 2005.

Starn, T. K., Shepson, P. B., Bertman, S. B., White, J. S., Splawn, B. G., Riemer, D. D., Zika, R. G., and Olszyna, K.: Observations of isoprene chemistry and its role in ozone production at a semirural site during the 1995 Southern Oxidants Study, J. Geophys. Res., 103(D17), 22 425–22 436, doi:10.1029/98JD01279, 1998.

Stroud, C., Madronich, S., Atlas, E., Cantrell, C., Fried, A., Wert, B., Ridley, B., Eisele, F., Mauldin, L., Shetter, R., Lefer, B., Flocke, F., Weinheimer, A., Coffey, M., Heikes, B., Talbot, R., and Bealer, D.: Photochemistry in the Arctic Free Troposphere: Ozone Budget and Its Dependence on Nitrogen Oxides and the Production Rate of Free Radical, J. Atmos. Chem., 47, 107–138, 2004.

Wayne, R. P., Barnes, I., Biggs, P., Burrows, J. P., Canos-Mas, C. E., Hjorth, J., LeBras, G., Moortgat, G. K.,Perner, D., Poulet, G.,Restelli, G., and Sidebottom, H.: The nitrate radical: Physics, chemistry and the environment, Atmos. Environ., 25, 1–206, 1991.

Zanis, P., Monks, P. S., Schuepbach, E., and Penkett, S. A.: On the relationship of HO_2+RO_2 with $j(O^1D)$ during the Free Tropospheric Experiment (FREETEX '96) at the Jungfraujoch Observatory (3580 m above sea level) in the Swiss Alps, J. Geophys. Res., 104, 26 913–26 925, 1999.

Table 1. Campaign air-mass sector-averaged chemical and physical parameters (1σ standard deviation given in brackets).

	NW	N	SW	W	S	NE	E
HO_2+RO_2/pptv	7.6 (6)	7.9 (4)	7.1 (6)	10.2 (8)	13.7 (10)	13.4 (10)	13.5 (7)
NO_x/pptv	151 (39)	73 (68)	111 (136)	63 (33)	230 (418)	275 (212)	352 (72)
NO/pptv	19 (47)	10 (14)	13 (12)	10 (7)	24 (55)	31 (21)	34 (26)
CH_4/ppbv	1813 (20)	1816 (32)	1785 (30)	1800 (13)	1821 (30)	1863 (50)	1925 (29)
CO/ppbv	90 (12)	81 (3)	77 (14)	83 (6)	82 (5)	112 (18)	149 (10)
H_2O_2/pptv	0.19 (0.19)	0.21 (0.14)	0.09 (0.07)	0.20 (0.10)	0.14 (0.05)	0.18 (0.11)	0.37 (0.10)
HCHO/ppbv	1.38 (0.18)	1.20 (0.08)	1.22 (0.17)	1.28 (0.26)	1.34 (0.12)	1.62 (0.22)	2.09 (0.17)
DMS/pptv	120 (98)	233 (66)	388 (264)	244 (227)	100 (107)	131 (88)	23 (24)
Isoprene/pptv	13 (24)	4 (1)	2 (1)	5 (6)	30 (61)	72 (119)	15 (26)
Benzene/pptv	29 (14)	24 (17)	20 (4)	27 (17)	18 (7)	62 (22)	114 (11)
Methanol/pptv	1068 (365)	852 (233)	1536 (384)	1086 (370)	1204 (291)	1747 (630)	1559 (596)

ACPD
5, 12313–12371, 2005

Table 2. Daylight-only (06:00 to 19:00) air-mass sector-averaged chemical and physical parameters (1σ standard deviation given in brackets).

	NW	N	SW	W	S	NE	E
HO_2+RO_2/pptv	10.6 (6)	9.6 (5)	8.5 (7)	15.1 (9)	16.4 (11)	21.0 (9)	17.4 (9)
NO_x/pptv	133 (256)	88 (77)	80 (39)	65 (30)	190 (497)	216 (112)	342 (93)
NO/pptv	31 (61)	16 (17)	15 (11)	13 (7)	34 (66)	43 (20)	57 (21)
CH_4/ppbv	1814 (22)	1818 (36)	1783 (30)	1799 (13)	1817 (29)	1852 (44)	1904 (29)
CO/ppbv	90 (12)	80 (3)	76 (15)	83 (5)	82 (5)	111 (18)	143 (8)
O_3/ppbv	33 (4)	28 (4)	25 (7)	26 (12)	20 (14)	33 (4)	39 (3)
$j(O^1D)\times10^{-6}/s^{-1}$	7.8 (7)	6.9 (6)	5.9 (6)	7.2 (5)	8.5 (6)	8.1 (6)	7.3 (8)
$N(O_3)$/ppbv h^{-1}	0.023 (0.2)	0.028 (0.1)	−0.019 (0.08)	0.025 (0.2)	0.087 (0.3)	0.51 (0.5)	0.47 (0.3)
H_2O_2/pptv	0.20 (0.2)	0.17 (0.1)	0.08 (0.1)	0.22 (0.1)	0.14 (0.04)	0.17 (0.1)	0.41 (0.08)
HCHO/ppbv	1.5 (0.2)	1.2 (0.1)	1.2 (0.1)	1.4 (0.3)	1.4 (0.2)	1.7 (0.2)	2.1 (0.2)

ACPD
5, 12313–12371, 2005

Table 3. Night-time-only (19:00–06:00) air-mass sector-averaged chemical and physical parameters (1σ standard deviation given in brackets).

	NW	N	SW	W	S	NE	E
HO_2+RO_2/pptv	4.2 (2)	5.6 (1)	4.4 (3)	4.1 (2)	6.4 (5)	7.7 (2)	10.5 (3)
NO_x/pptv	174 (521)	59 (57)	152 (200)	61 (36)	301 (214)	344 (274)	359 (54)
NO/pptv	4.8 (3)	4.7 (4)	9.6 (13)	6.1 (6)	4.9 (3)	17.0 (12)	15.2 (8)
CH_4/ppbv	1813 (17)	1814 (28)	1787 (31)	1802 (14)	1827 (33)	1877 (53)	1941 (16)
CO/ppbv	90 (13)	81 (2)	78 (12)	84 (6)	81 (3)	113 (19)	154 (11)
O_3/ppbv	32 (4)	30 (2)	26 (8)	22 (12)	28 (6)	31 (3)	40 (2)
NO_3/pptv	4.7 (2)	5.9 (3)	nd	4.5 (2)	2.7 (1)	5.7 (5)	11.7 (6)
HCHO/ppbv	1.28 (0.16)	1.16 (0.05)	1.25 (0.23)	1.14 (0.17)	1.33 (0.07)	1.54 (0.23)	nd
Alkenes/pptv	60 (48)	33 (11)	71 (57)	64 (30)	71 (47)	187 (141)	188 (82)

nd: no data

ACPD
5, 12313–12371, 2005

Table 4. Sensitivity of the Model/Measurement (HO_2 + ΣRO_2) agreement for varying chemical complexity.

Model Run[a]	Model/Measurement
$CO+CH_4$ chemistry (Het with IO chemistry) – constrained to measurements of CO and CH_4	3.3±1.8
Full Chemistry (Het with IO chemistry) – constrained to measurements of CO, CH_4, 23 hydrocarbons and chloroform	2.6±1.3
Full+Oxy – constrained to measurements of CO, CH_4, 23 hydrocarbons, chloroform and 3 oxygenates	2.5±1.3
Full+Oxy (Het with IO chemistry) – constrained to measurements of CO, CH_4, 23 hydrocarbons, chloroform and 3 oxygenates	2.3_{41}±1.2
Full+Oxy+Per (Het with IO chemistry) – constrained to measurements of CO, CH_4, 23 hydrocarbons, chloroform, 3 oxygenates and 2 peroxides	2.3_{43}±1.2

[a] Full details of model runs in Sommariva et al. (2005); Het with IO chemistry – model additionally constrained to measured IO and j(HOI) using a transition regime expression to calculate the heterogeneous uptake of the gas-phase species.

ACPD
5, 12313–12371, 2005

Table 5. Daily $N(O_3)$ maxima and minima and campaign average in EASE 97, SOAPEX 2 and NAMBLEX (all in ppbv h^{-1}).

Campaign and Season	Season	Mean
Mace Head (EASE 96[a])	Summer	0.3
Mace Head (EASE 97[a])	Spring	1.0
Cape Grim (SOAPEX 2[b])	Summer	−0.01
N. Pacific (PHOBEA[c])	Spring	−0.1
E. Pacific (ORION99[d])	Summer	0.2–3.4
Mace Head (NAMBLEX[e])	Summer	0.11

[a] see Salisbury et al. (2002), [b] see Monks et al. (2005), [c] Kotchenruther et al. (2001), [d] Kanaya et al. (2002), [e] this work.

ACPD
5, 12313–12371, 2005

Table 6. Sensitivity of derived $P(O_3)$ and $L(O_3)$ to NO from a series of marine boundary layer campaigns.

	$d\ln(P(O_3))/d\ln(NO)$	$d\ln(L(O_3))/d\ln(NO)$
Cape Grim(SOAPEX 2[a])	0.90	0.06
Mace Head (EASE 97[b])	1.10	0.27
Weybourne (winter[c])	0.92	0.02
Weybourne (summer[c])	0.95	0.28
Mace Head (NAMBLEX[d])	1.0	0.62

[a] data from Monks et al. (2005); [b] data from Salisbury et al. (2002); [c] data from Fleming et al. (2005); [d] this work.

ACPD
5, 12313–12371, 2005

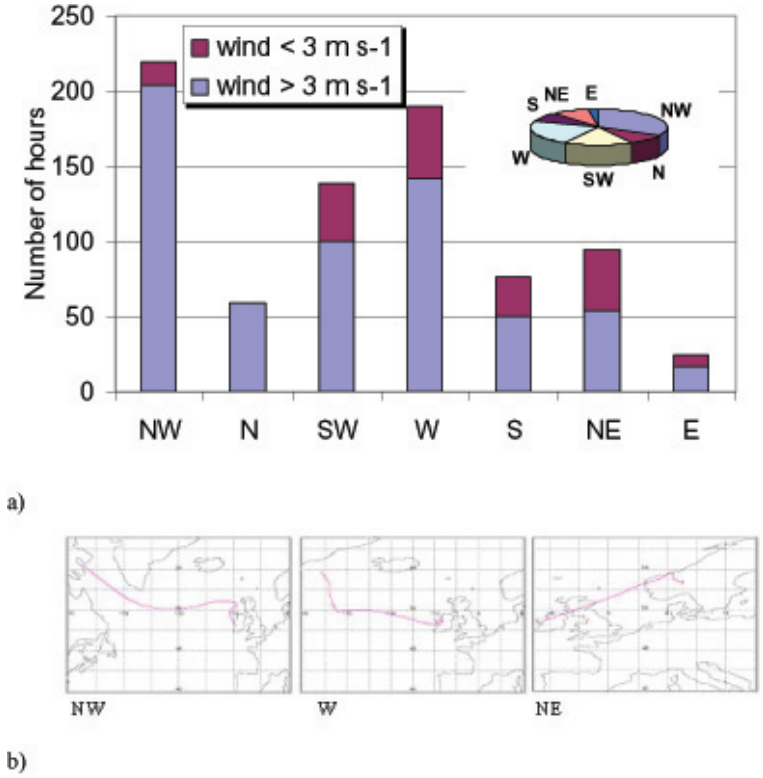

Fig. 1. (a) Air-mass sector divisions for winds less than and greater than $3\,m\,s^{-1}$ and inset pie-chart of percentage divisions between sectors (winds $>3\,m\,s^{-1}$); **(b)** Typical back-trajectories for the NW, W and NE air-mass sectors.

ACPD

5, 12313–12371, 2005

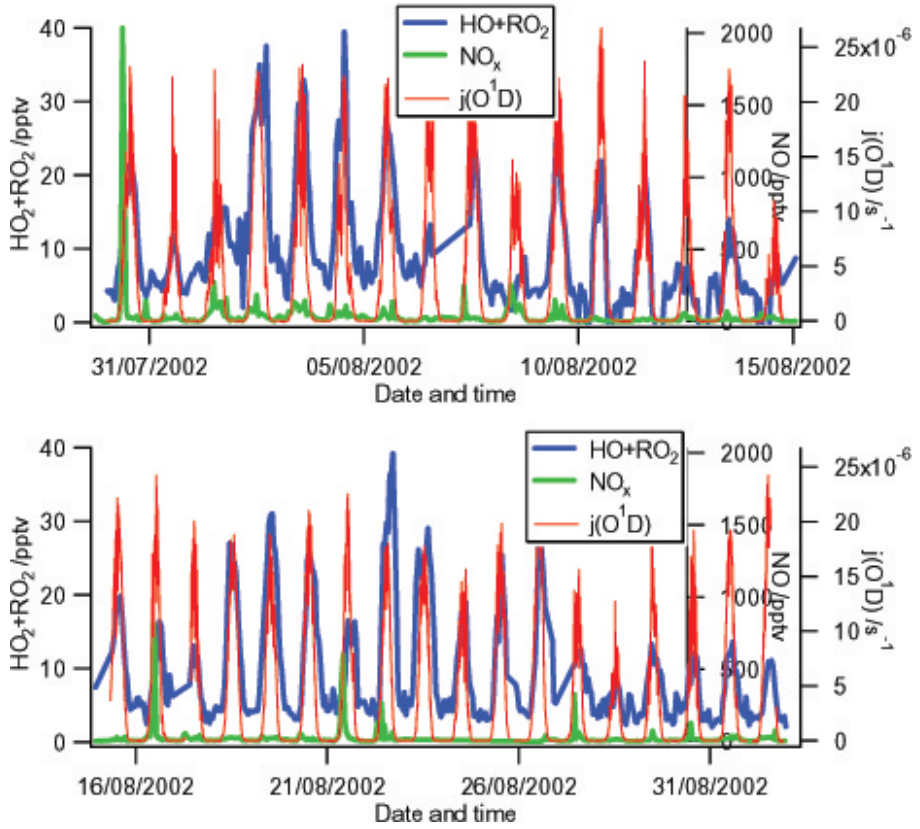

Fig. 2. $[HO_2+\Sigma RO_2]$, $j(O^1D)$ and $[NO_x]$ campaign time series.

ACPD
5, 12313–12371, 2005

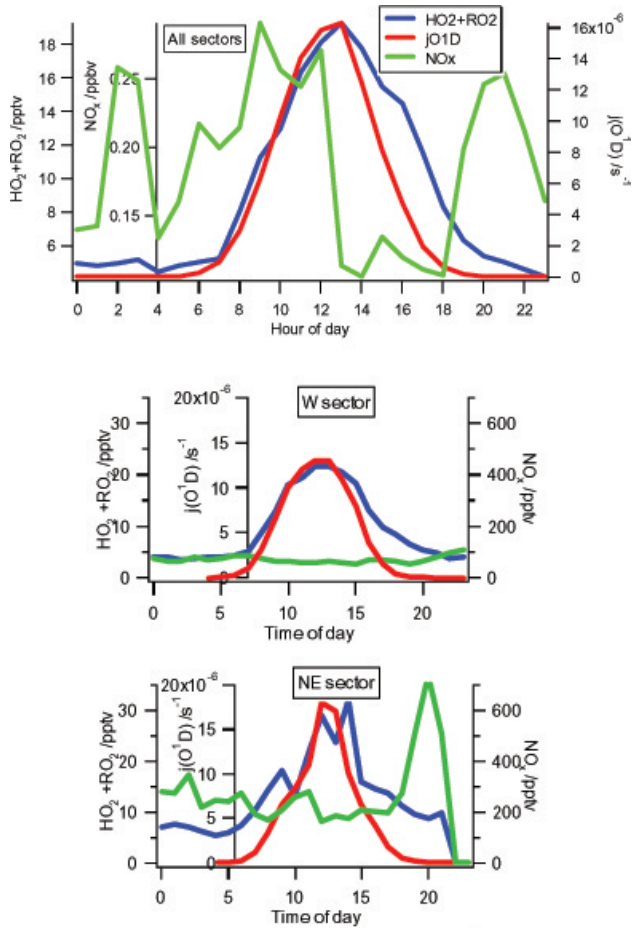

Fig. 3. Hourly-averaged $[HO_2+\Sigma RO_2]$, $[NO_x]$ and $j(O^1D)$ diurnal cycles for campaign data and W and NE air-mass sector averages.

ACPD
5, 12313–12371, 2005

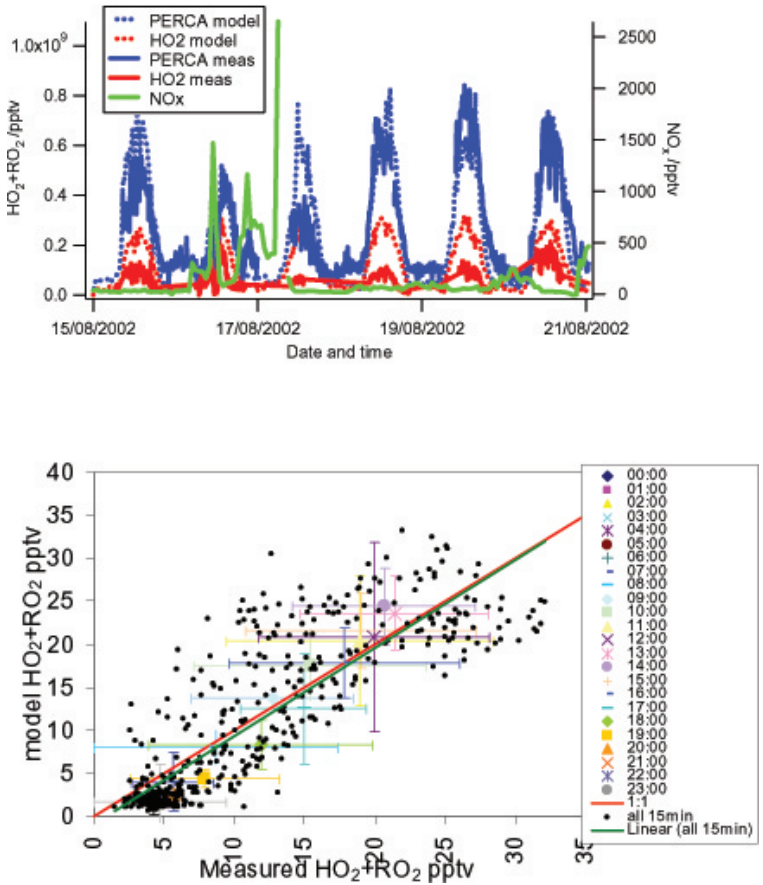

Fig. 4. (a) Measured and modelled PERCA [$HO_2 + \sum RO_2$] and FAGE [HO_2]; **(b)** MCM modelled vs. measured [$HO_2 + \sum RO_2$] (15-min data) and hourly-averaged data.

ACPD
5, 12313–12371, 2005

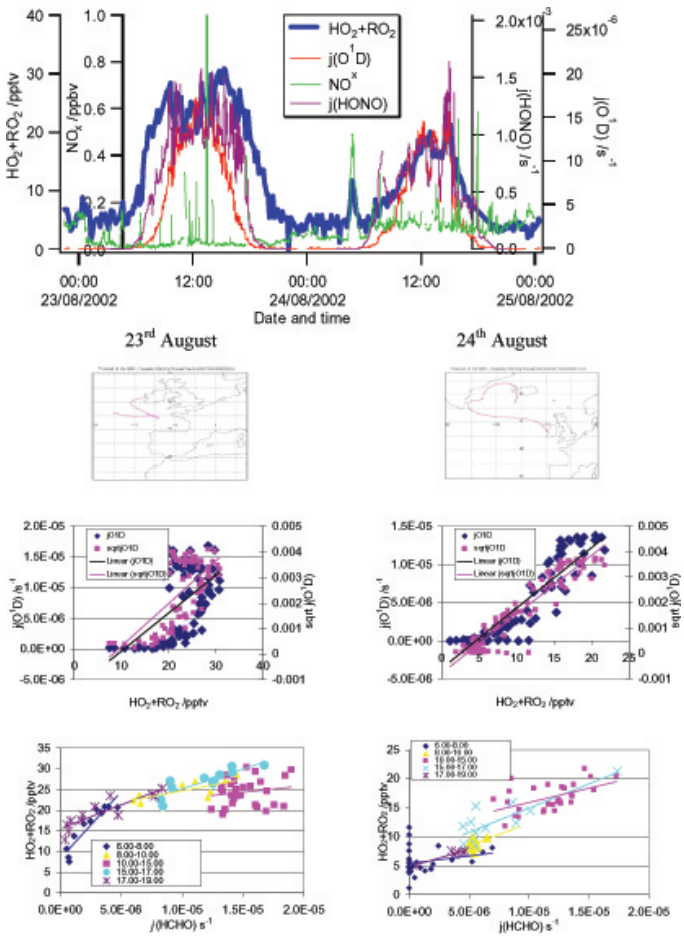

Fig. 5. 23 and 24 August $HO_2+\sum RO_2$ and $j(O^1D)$ diurnal cycles and five-day back-trajectories. $j(O^1D)$ and $\sqrt{j(O^1D)}$ vs. $[HO_2+\sum RO_2]$ linear regressions and $[HO_2+\sum RO_2]$ vs. j(HCHO) trends at different periods of the day are shown beneath the back-trajectories.

ACPD
5, 12313–12371, 2005

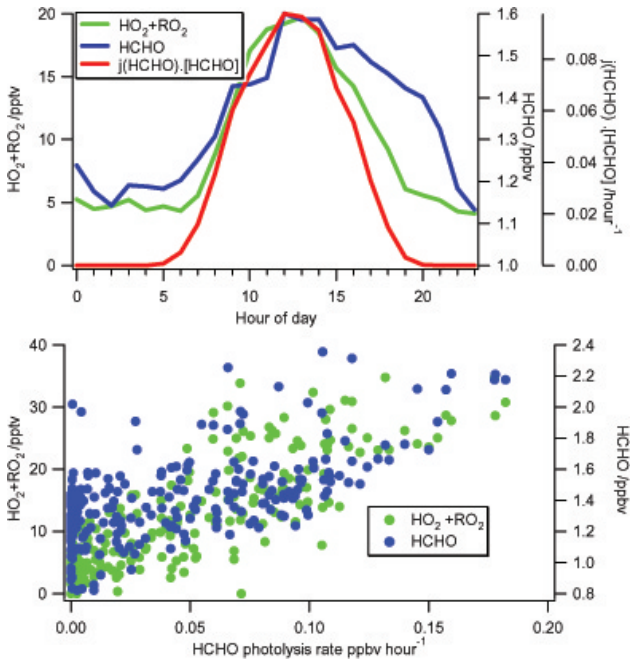

Fig. 6. **(a)** Hourly-averaged diurnal cycle of [HCHO], [HO_2+RO_2] and j(HCHO)×[HCHO]h^{-1} **(b)** Trend of ten minute-averaged [HO_2+RO_2] and [HCHO] vs. j(HCHO)×[HCHO].

ACPD
5, 12313–12371, 2005

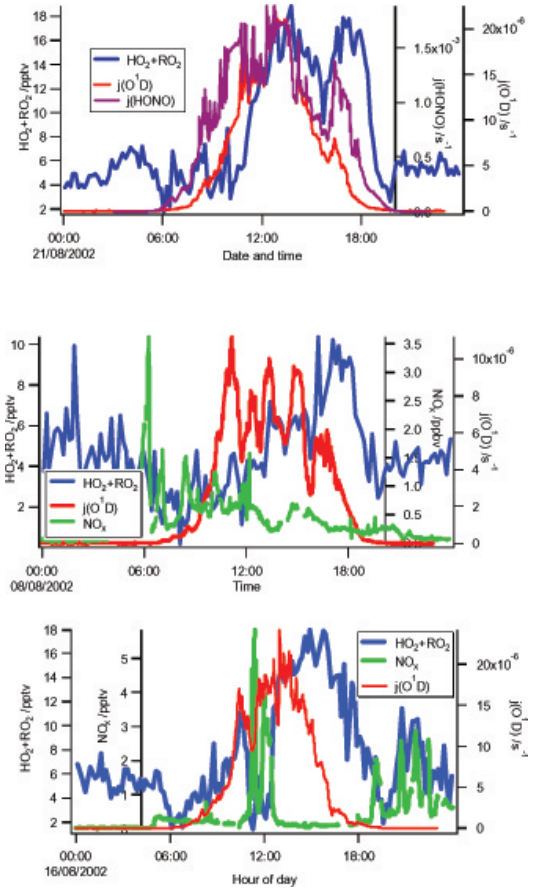

Fig. 7. Case study days: **(a)** 21 August, **(b)** 16 August, **(c)** 8 August $[HO_2 + \sum RO_2]$, $j(O^1D)$ (and $[NO_x]$ or j(HONO)) diurnal cycles.

ACPD
5, 12313–12371, 2005

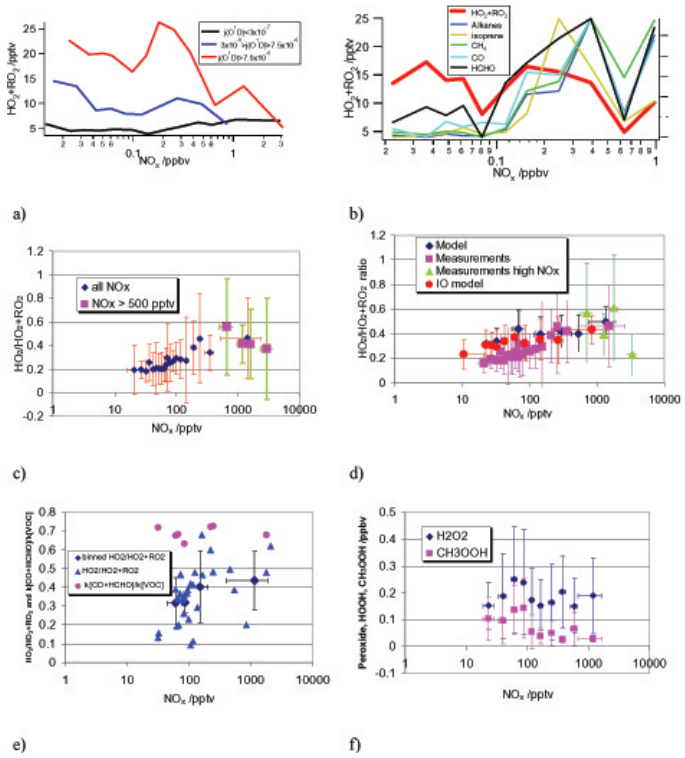

Fig. 8. (a) 10 min-averaged $[HO_2+\sum RO_2]$ vs. $[NO_x]$ at three light intensity regimes; **(b)** Hourly-averaged daylight (06:00–19:00) [VOCs], [CO] and $[HO_2+\sum RO_2]$ vs. $[NO_x]$. The right-hand axis is an amalgamation of a scaled axis for all of CO, CH_4, HCHO, isoprene and alkanes for comparison purposes; **(c)** $HO_2/(HO_2+\sum RO_2)$ vs. $[NO_x]$: 15 min-averaged data with values at $[NO_x]$>500 pptv in smaller bins; **(d)** Measured and modelled $HO_2/(HO_2+\sum RO_2)$ ratios vs. $[NO_x]$ for hourly-averages (Model days: 1, 2, 9, 10, 15–22, 31 August and 1 September – model runs both full-oxy with and without halogens (see Table 4)); **(e)** Hourly-averaged $HO_2/(HO_2+\sum RO_2)$ and ϕ(CO+HCHO) vs. $[NO_x]$; **(f)** Hourly-averaged [peroxide] vs. $[NO_x]$.

ACPD
5, 12313–12371, 2005

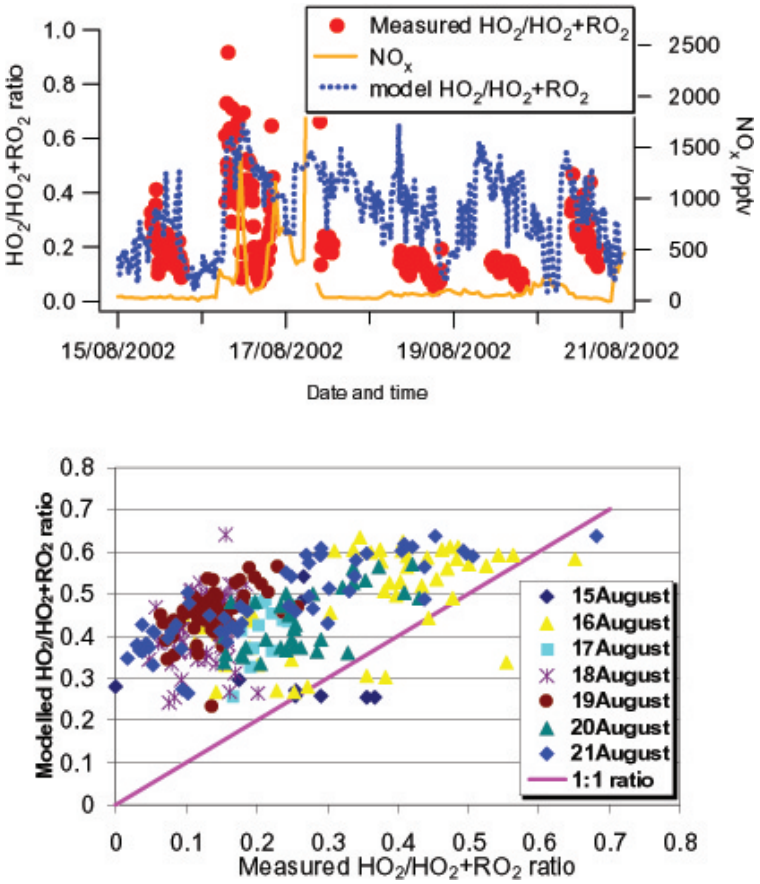

Fig. 9. **(a)** Hourly-averaged measured and modelled [HO_2+RO_2] diurnal cycles for the 15–22 August **(b)** Measured and modelled HO_2/HO_2+RO_2 ratios for 15–21 August.

ACPD
5, 12313–12371, 2005

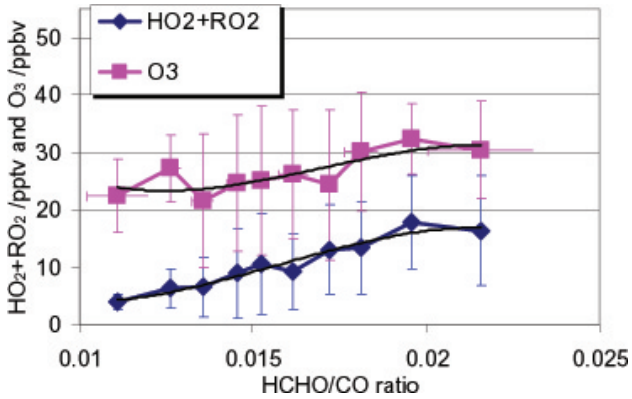

Fig. 10. Hourly-averaged [HO_2+RO_2] and [O_3] vs. [HCHO]/[CO] fitted with a third order polynomial.

ACPD
5, 12313–12371, 2005

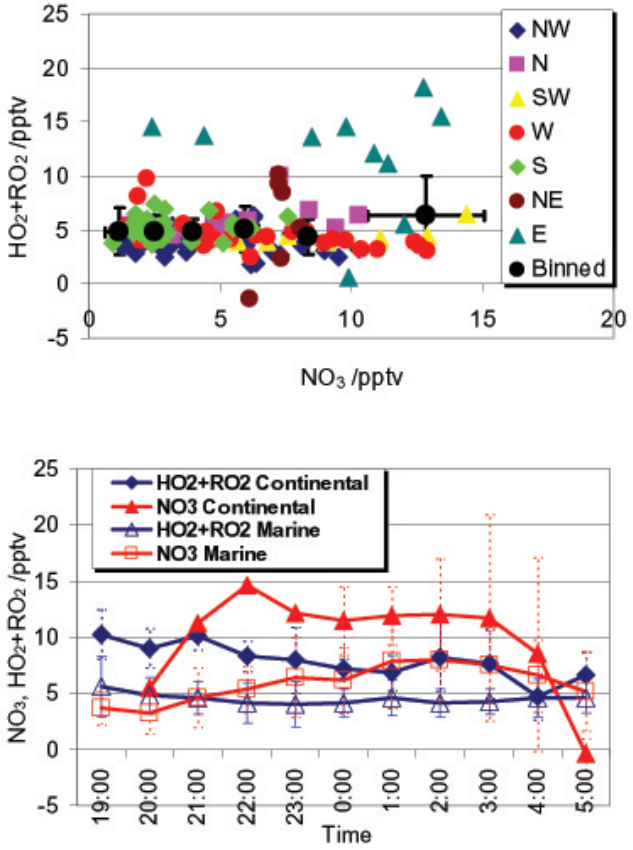

Fig. 11. **(a)** Hourly-averaged $[HO_2+RO_2]$ vs. $[NO_3]$ for air-mass sectors. Large blue markers represent all hourly-averaged concentrations divided into six NO_3 bins and corresponding standard deviations **(b)** $[NO_3]$ and $[HO_2+RO_2]$ at night (19:00 to 06:00).

ACPD
5, 12313–12371, 2005

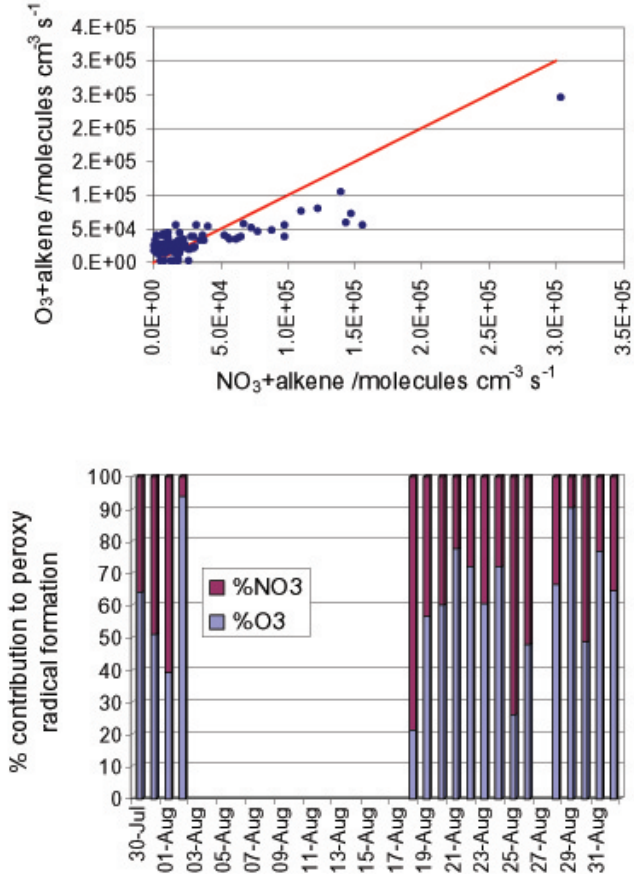

Fig. 12. (a) Flux of peroxy radicals formed from alkene-NO_3 and alkene-O_3 channels: Hourly-averaged night-time (19:00 to 06:00) fluxes. The red-line is the 1:1 ratio; **(b)** Percentage contribution of O_3 and NO_3 to peroxy radical formation from alkene night-time reactions.

ACPD
5, 12313–12371, 2005

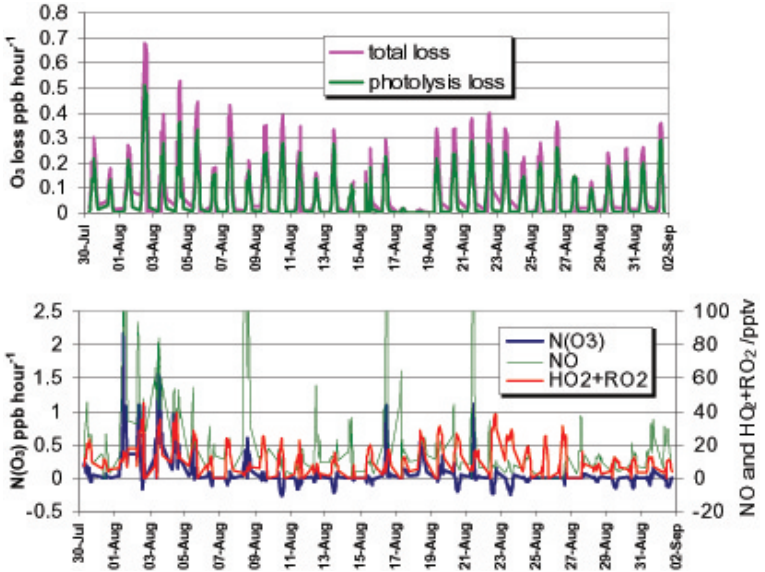

Fig. 13. **(a)** Total ozone loss and ozone loss via photolysis **(b)** Net ozone production and corresponding [NO] and [HO_2+RO_2] used to calculate P(O_3).

ACPD
5, 12313–12371, 2005

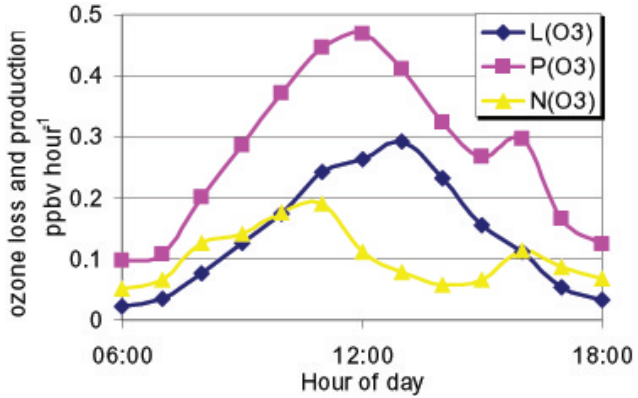

Fig. 14. Campaign hourly-averaged loss, production and net ozone production.

ACPD
5, 12313–12371, 2005

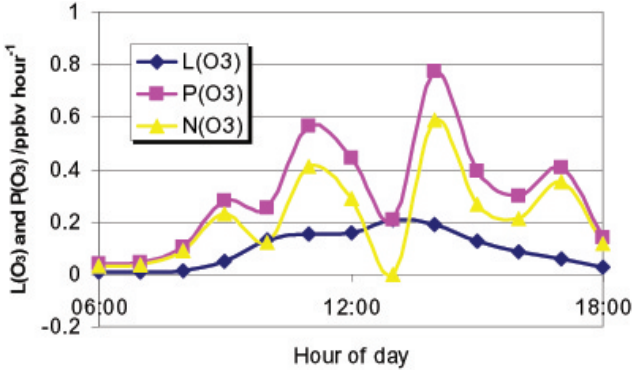

Fig. 15. Case day 8 August: Ozone production, loss and net production.

ACPD
5, 12313–12371, 2005

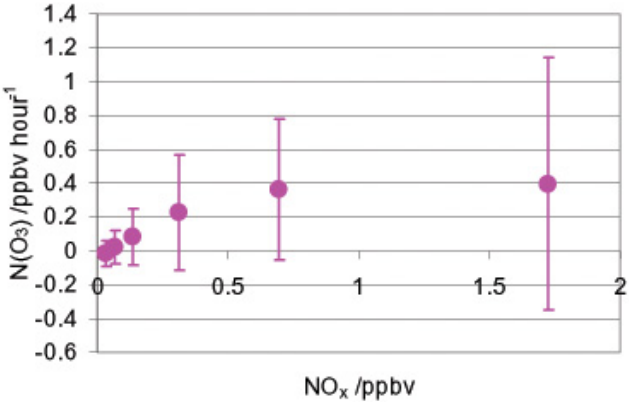

Fig. 16. Net ozone production for daylight hours binned according to [NO_x].

ACPD
5, 12313–12371, 2005

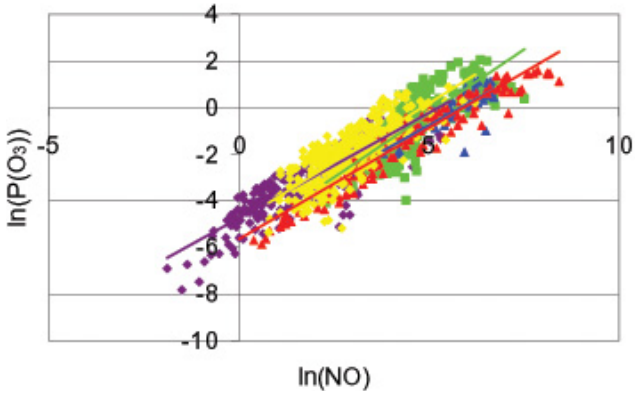

Fig. 17. ln($P(O_3)$) vs. ln(NO) for Weybourne summer (red) and winter (blue), Mace Head; NAMBLEX (yellow), EASE 97 (green) and Cape Grim; SOAPEX 2 (purple). See Table 6 for campaign details.

ACPD
5, 12313–12371, 2005